吉林大学仪器科学与电气工程学院

College of Instrumentation & Electrical Engineering, Jilin University

科技学术实践“六个一”训练项目

Academic Practice “Six in One” Training Project

论文集
Proceedings

2019 年下半年

2019（Second Half）

目录

CONTENTS

第一部分　中文论文集

PART I　CHINESE PROCEEDINGS

UWB 定位的智能小车避障技术研究*

尚虎军；王志颖；李志鑫

（吉林大学 仪器科学与电气工程学院　长春 130021）

摘要：随着工业自动化程度的不断提高以及基于位置服务需求的增加，定位导航技术进入了一个飞速发展的时代。利用无线通信技术进行室内定位已经成为导航技术研究的一个热点。本文以小车为研究对象，对其室内定位、无线视频传输和避障技术进行了研究。构建了一个由一标签、三基站组成的室内超宽带无线定位系统，利用 TOF 方法测距从而实现自主定位。研究了超声波与红外相结合的多传感器避障技术与算法，在避障算法方面通过障碍物和小车的位置关系确定避障方向。借助 WIFI 通信技术实现树莓派与上位机之间的视频传输。开发了上位机软件显示小车位置坐标以及传输的视频。

关键词：导航技术　视频传输　超宽带定位　多传感器避障

Research on Intelligent Car Based on Raspberry Pi and UWB Technology

SHANG Hujun；WANG Zhiying；LI Zhixin

（Jilin University,College of Instrumentation &Electrical Engineering,Changchun 130021,China）

Abstract： With the development of industrial automation and the increasing demand for location-based services, positioning and navigation technology has entered an era of rapid development. Using wireless communication technology for indoor positioning has become a hotspot of navigation technology research. In this paper, the indoor positioning, wireless video transmission and obstacle avoidance technology of the car were studied. An indoor UWB wireless positioning system composed of one tag and three base stations is constructed, and the location is realized by TOF method. The multi-sensor obstacle avoidance technology and algorithm based on the combination of ultrasonic and infrared are studied. In the aspect of obstacle avoidance algorithm, the direction of obstacle avoidance is determined by the position relationship between obstacle and car. Video transmission between raspberry pie and host computer is realized by means of WIFI communication technology. The upper computer software is developed to display the car position coordinates and the transmitted video.

Key words： Navigation technology　Video transmission　UWB positioning　Multi-sensor obstacle avoidance

0　引言

随着大型商场、各种工厂等大型场馆的建立，室内定位及导航需求日趋强烈，本文利用 UWB 室内定位技术，首先通过 TOF 算法测距，然后通过三边定位算法实现智能小车的室内定位[1-3]。搭建了超声波与红外结合的多传感器硬件避障平台，并通过车载摄像头与终端之间的无线视频传输来实时监控小车周围的环境信息。小车在行驶过程中可以自主避障，操作人员在上位机界面可以监视小车的实时位置及周围环境状况。

1　总体设计方案

本设计的研究内容包括 UWB 定位原理、避障系统的软硬件设计、WIFI 通信及上位机显示。总体的设计方案如图 1 所示。

* 指导老师：刘通

项目类型：大学生创新训练项目（2018B6518）

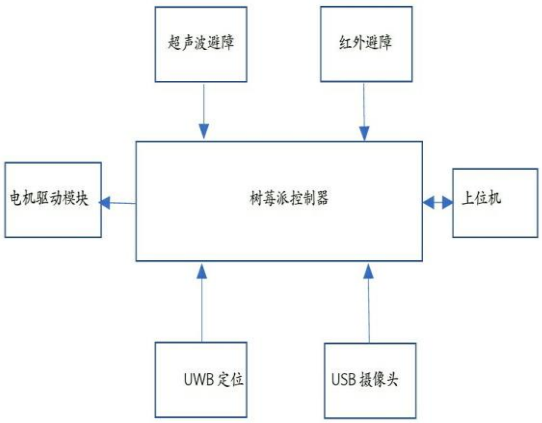

图 1 总体方案设计图

Figure 1 Overall scheme design

本设计需要达到的目标如下：

（1）将车载摄像头拍摄的视频利用 WIFI 实时传输到上位机并显示；

（2）采用 UWB 定位，在上位机显示出小车所在位置的实时坐标；

（3）小车可以应用超声波结合红外传感器避障模块自主躲避障碍物。

2 系统实现的关键技术及难点

2.1 UWB 室内定位

UWB（Ultra Wideband）是一种无载波通信技术，利用纳秒至微微秒级的非正弦波窄脉冲传输数据。通过在较宽的频谱上传输极低功率的信号，UWB 能在 10 米左右的范围内实现数百 Mbit/s 至数 Gbit/s 的数据传输速率。超带宽系统与传统的窄带系统相比，具有穿透力强、功耗低、抗多径效果好、安全性高、系统复杂度低、能提供高精确度的定位等优点。因此，超带宽技术可以应用于室内静止或者移动物体以及人的定位与导航，且能提供十分精确的定位精度[4]。

UWB 定位算法主要包含两部分，首先是采用 TOF 测距算法获取标签到固定基站之间的距离，然后再根据三边定位算法得到标签坐标。

（1）TOF 测距

DWM1000 超宽带测距，使用的是 TOF（time of fly）测距方式，也就是计算无线电磁波传输时间，通过传输的时间换算成距离。一共有两个设备，也就是两个 DWM1000 模块，即基站和标签。标签在 t_A 时刻发送一条信息给基站，经过空中一段时间 t_1 传播在时刻 t_B 到达基站。基站收到标签的信息后，经过一段时间 t_2，在时刻 t_C 时将回复信息发送到标签，这个信息经过一段时间 t_1 后，在 t_D 时刻标签收到。如 2 图所示：

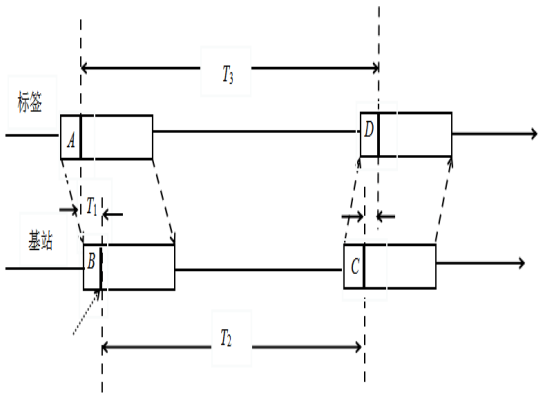

图 2 TOF 测距原理图

Figure.2 TOF ranging principle

标签通过读寄存器获得 t_A 时刻和 t_D 时刻时间戳记

$$t_3=t_D-t_A;$$

从上图我们还可以看到另外一个时间 t_2，这个时间长度实际是在标签中计算获得的。基站发送给标签的信息包含了自己接收信息时刻 B 的时间戳以及发送信息时刻 C 的时间戳，当标签收到信息后二者减法即可得到 t_2

即 $t_2=t_C-t_B$；

不同的设备时钟频率是一致的，故两次无线信号传输的时间

$$t=t_3-t_2;$$

可得基站与标签之间的距离为

$$d=v*t/2$$

（2）三边定位算法

经过 TOF 测距已经测得标签距离三个基站的距离,应用三边定位算法可以根据这多个距离计算出标签的二维坐标。

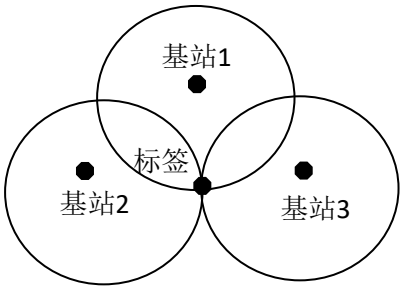

图 3 三边定位原理图

Figure.3 Principle of trilateral positioning

假设三个基站物理坐标为（x_1,y_1），（x_2,y_2）和（x_3,y_3），未知的标签坐标为（x,y）,标签到基站的测距为 d_1,d_2,d_3,则有方程组

$$（x-x_1）^2+（y-y_1）^2=d_1^2$$

$$（x-x_2）^2+（y-y_2）^2=d_2^2$$

$$（x-x_3）^2+（y-y_3）^2=d_3^2$$

上边方程组为非线性方程组，用方程组中前 n-1 个方程减去第 n 个方程后，得到线性化的方程：

$$AX=b$$

其中：

$$A=\begin{bmatrix}2(x_1-x_3) & 2(y_1-y_3)\\ 2(x_2-x_3) & 2(y_2-y_3)\end{bmatrix}$$

$$b=\begin{bmatrix}x_1^2-x_3^2+y_1^2-y_3^2+d_3^2-d_1^2 & 2(x_1-x_3) & 2(y_1-y_3)\\ x_2^2-x_3^2+y_2^2-y_3^2+d_3^2-d_1^2 & 2(x_2-x_3) & 2(y_2-y_3)\end{bmatrix}$$

用最小二乘法解得

$$X=(A^TA)^{-1}A^Tb$$

2.2 超声波结合红外避障设计

此设计采用超声波避障模块作为主要避障部分，由于超声波测距有 0-2cm 的测距盲区，因此增加了红外开关模块来辅助避障。超声波测距使用的是 HC-SR04 测距模块，可以提供 2cm-400cm 的非接触式距离感测功能，测距精度可达 3mm。

采用检测往返时间来确定小车与障碍物之间的距离，原理是收集从超声波发射器发出的超声波，经过障碍物的反射，到接收器接收到超声波所用的时间即往返时间。往返时间除以 2 再乘以超声波在空气中传播的速度，就是小车与障碍物之间的距离[5-6]。

超声波测距传感器在舵机的转动下，循环检测前方、左方和右方 3 个方向的障碍物距离，小车以离三个方向障碍物的距离以及红外探头的反馈为判据对行驶路径做出判断，使小车能自主避障行驶[7]。设计超声波测距与红外传感器结合的避障算法，算法流程图如图 4 所示。行进过程中，首先用超声波检测正前方障碍物距离，如果距离大于 30cm 则继续向前行驶，并用红外辅助避障检测可能出现在超声波测距盲区里的障碍物进行躲避；如果距离前方障碍物小于 15cm 则向后，如果距离在此之间则通过舵机旋转检测小车左方和右方的障碍物距离。如果左右两侧的距离均小于安全距离 15cm，则小车后退；否则若右侧距离大于左侧距离，则小车右转，反之则左转。

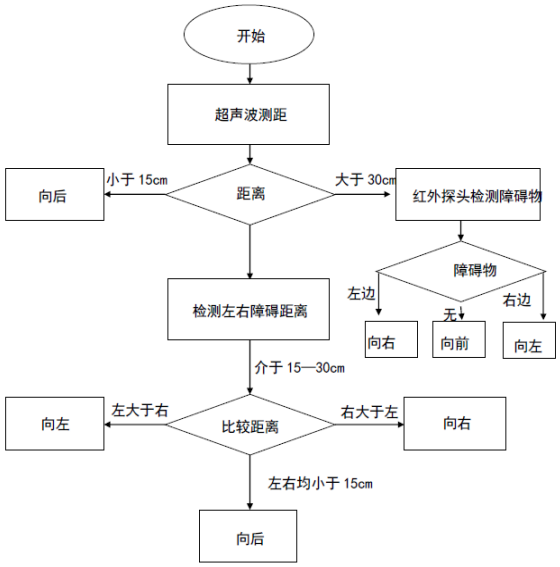

图 4　避障算法流程图

Figure.4　Flow chart of obstacle avoidance

超声波避障技术的难点：受制于其自身避障技术的特点，无法保证在各种类型的场景下都能正常工作，这就需要不断的实验和试错，并且持续的优化算法，保证各类场景下都能正常工作，不会给出错误的指令[8]。

2.3 远程视频监控功能

此功能使用支持 Linux 系统的开源软件 mjpg－streamer 作为视频监控软件，利用 USB 摄像头对小车周围环境状况进行视频图像的采集，并通过 WIFI 网络与 PC 机通信，实现对周围环境的实时无线监控[9]。

mjpg－streamer 是基于 IP 地址的视频流服务器，采用内存映射方式[10-11]。通过对终端命令的分析，由输入插件 input_uvc. so 把兼容 Linux－UVC V4L2 设备中拍摄的视频分解成独立的 jpeg 图像数据，并放入到内存中；由多个输出插件处理这些视频数据；由输出插件 output_http. so 负责把内存中的视频数据取出并传输到网页上显示。

3　系统测试结果

3.1 小车整体结构

基于树莓派控制器的智能小车整体实物图如图 5 所示。此智能小车由供电系统、控制系统、驱动系统、定位系统、自主避障系统和视频传输系统等组成。

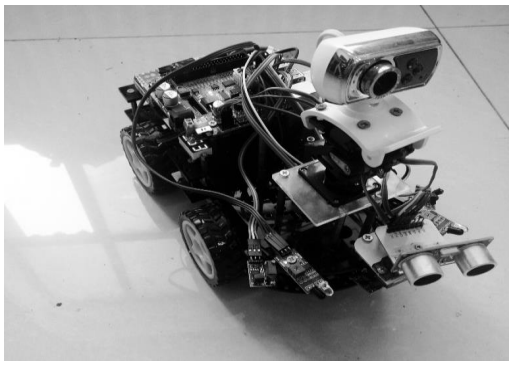

图 5　小车俯视图

Figure.5　Top view of the car

3.2 系统测试

基于树莓派控制器的智能小车最终实现的功能有：自主定位并显示位置坐标、无线视频传输至终端、利用超声波结合红外传感器实现自主避障。主要测试内容如下：

（1）自主定位测试，在终端打开坐标显示界面可以显示在以主基站为原点所建坐标系中标签（小车）的位置坐标，如图 7 所示；定位测试结果如下表一所示。

表 1　UWB 定位系统测试结果

Table 1　test results of UWB positioning system

位置编号	实际坐标（cm）	平均测量坐标（cm）	距离误差（cm）
1	(60,60)	(65,67)	8.54
2	(60,120)	(66,108)	13.42
3	(120,120)	(127,110)	12.21
4	(180,120)	(182,107)	13.15
5	(180,180)	(190,168)	15.62
6	(240,240)	(238,252)	12.16

（2）视频传输测试，打开上位机视频显示界面可以看到车载摄像头实时拍摄的视频，小车行驶过程中视频较为清晰流畅，采用桌面计时器测得视频显示延迟约为 0.38 秒。如图 6 所示

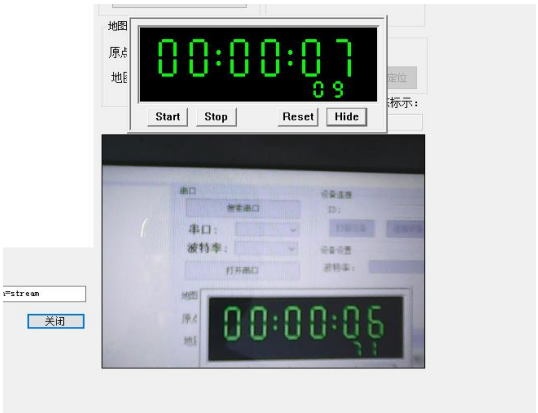

图 6　视频延迟测试

Figure.6　Video delay testing

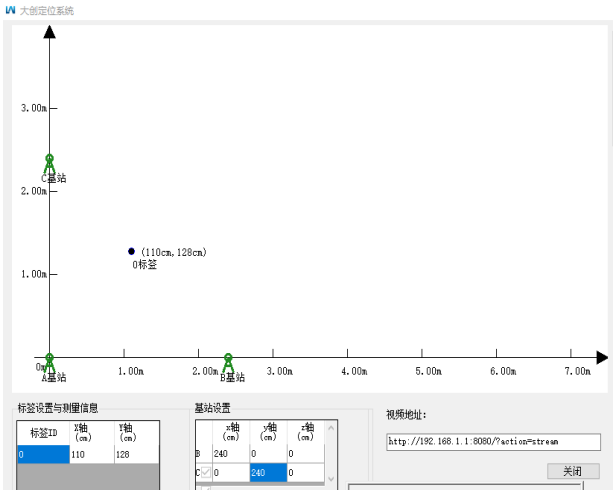

图 7　上位机坐标显示界面

Figure.7　Coordinate display interface

（3）自主避障测试，将小车放在置有一定障碍物的平面内，在行驶过程中遇到障碍物时小车可以安全制动，并根据与障碍物的相对位置来躲避障碍物继续行驶，可见小车自主避障功能正常。

4　结论

本文设计了基于树莓派控制器的智能小车系统，详细介绍了 TOF 测距方法与原理、三边定位算法及其求解、超声波避障原理以及无线视频传输方案。通过不断调试基本实现了小车预设目标的所有功能，能够实时显示小车的坐标，通过视频传输功能可以对小车周围的环境状况进行实时监控，且视频较为清晰流畅，在小车行进过程中可以自主躲避行进方向上的障碍物。

参考文献

[1]　李龙委,胡海燕,章仁辉,李春光,孙立宁.基于 UWB 室内定位的迎宾机器人系统研究[J].机械与电子,2018,36（12）:58-63+68.

[2]　范烨,陈秋霞,倪丽慧.DWM1000 模块的 UWB 机器人室内定位系统[J].单片机与嵌入式系统应用,2018,18（11）:48-50+54.

[3]　曾贵苓,王苹,张玉明,段争光.基于 UWB 的智能搬运小车[J].湖北民族学院学报(自然科学版),2019,37(02):223-227.

[4]　李威,叶焱,谢晋雄,刘太君.UWB 高精度室内定位系统及实现[J].数据通信,2018（05）:13-18.

[5] 马铎,党小娟,张慧.超声波智能避障小车的设计与实现[J].企业科技与发展,2018（09）:87-88.

[6] 邢强,虞凯西,谷玉之.基于测距超声波传感器的间距平衡避障策略[J].现代电子技术,2018,4（20）:97-99+103.

[7] 吴波涛,孔金平,王湘.基于 Arduino 和树莓派的智能小车的设计与实现[J].电子设计工程,2017,25(15):58-61.

[8] 李雯雯. 基于多种传感器的自动导航小车避障的研究[D].西安科技大学,2008.

[9] 刘洪波,郑少伟,谢宇希,王金江,唐钦.嵌入式无线视频小车的设计与实现[J].价值工程,2017,36(28):138-139.

[10] 胡志超,孔锦明,魏豪特.基于树莓派的移动监控小车设计[J].科技广场,2017(12):78-80.

[11] 邱绪林.基于 wifi 的无线视频传输系统[J].中国新通信,2017,19（04）:31.

电路延时及频率测量装置的设计*

张成刚；高　兴；刘　赫

（吉林大学 仪器科学与电气工程学院，长春 130021）

摘要：电路延时及频率测量装置以 STM32 为主控制器，通过波形调理电路把模拟量转化成数字量，结合 FPGA 对输入信号进行精确延时，延时间隔步进值小于 10ns，步进程控可调。频率测量采用定时计数法，利用锁相环把 FPGA 的基准时钟源倍频至 200MHz，设定的闸门时间为 0.5s。FPGA 与主控制器通过 SPI 通信，主控制器经过解码和数据运算后得出待测信号的频率。在题设要求的频带范围内，测频相对误差不大于 2.1%，从而达到对电路进行精确延时以及频率测量，并将输入信号、延时信号以曲线的形式显示。

关键词：有效值检波　延时电路　频率测量　SPI 通信

Design of Circuit Delay Measurement Device

Zhang Chenggang；Gao Xing；Liu He

（Jilin University,College of Instrumentation &Electrical Engineering,Changchun 130021,China）

Abstract: The circuit delay and frequency measuring device uses STM32 as the main controller, and converts the analog quantity into digital quantity through the waveform conditioning circuit, and combines the FPGA to accurately delay the input signal. The delay interval step value is less than 10 ns, and the step process control is adjustable. . The frequency measurement uses the timing counting method. The phase-locked loop is used to multiply the reference clock source of the FPGA to 200MHz, and the set gate time is 0.5s. The FPGA communicates with the main controller through SPI, and the main controller obtains the frequency of the signal to be tested after decoding and data calculation. In the frequency range required by the title, the relative error of the frequency measurement is not more than 2.1%, so as to achieve accurate delay and frequency measurement of the circuit, and display the input signal and the delayed signal in the form of a curve.

Key words: RMS detection　delay circuit　frequency measurement　SPI communication

0　前言

信息化时代的到来，延时和频率测量在国家的众多领域都有广泛的应用。例如政治、军事、科技、经济。频率测量系统在工业控制、交通运输、电子信息等领域均有十分广泛的应用。计时、工业控制领域、定位导航、数字化技术和计算机都离不开频率测和量控制技术[1]。

常用的频率测量方法有定时计数法和等精度测量法等方式[2]，等精度测量法适用于频率变化范围大的场合，真正测频开始的时间为同步闸门开启时间，其与系统时钟和被测信号同步，频率大小不影响测频产生的误差。经过计算±1 误差可知，定时计数法测频低频段误差在允许范围内，因此采用此种方法测频。

延时模块可采用模拟方法 RC 电路进行延时，但是此种延时方法无法做到延时时间程控可调，且延时时间难以严格的控制。利用调理电路把模拟信号转化为数字信号，然后利用 FPGA 进行单位步进值延时，通过多个步进值的叠加，实现长时间的延时功能，还可以满足系统的延时精度要求。

1　检波电路方案设计

利用 AD8361 芯片实现有效值检波：AD8361

* 指导老师：千承辉

项目类型：学科竞赛 2018 年吉林省大学生电子设计竞赛 A 题

是真有效值响应功率检波器，适用于高频信号，检波范围为 LF-2.5GHz，最大非线性失真度± 0.25dB。其优势在于能够测量各种复杂波形的有效值而不必考虑波形失真程度，可单电源供电，功耗低。

电压的有效值定义为

$$U_{\text{rms}}=\sqrt{\frac{1}{T}\int_0^T U^2(t)\,dt} \qquad ①$$

因此，为了获得均方根响应，必须有平方律检波的伏安特性[3]。该幅频特性测试装置使用集成检波芯片 AD8361 进行检波，输出为代表输入信号有效值的直流电压，根据正弦波的波峰系数换算为输入信号的峰峰值

$$V_{p-p}=2.828U_{\text{rms}} \qquad ②$$

有效值检波电路如图 1 所示。输入使用 ADA4817 进行缓冲，其中用是避免前级放大器的输出特性被负载变动所影响，AD8361 检波器的输出端后接 RC 电路。利用一阶 RC 电路进行抗混叠滤波，输出信号送入 ADC 进行电压采集

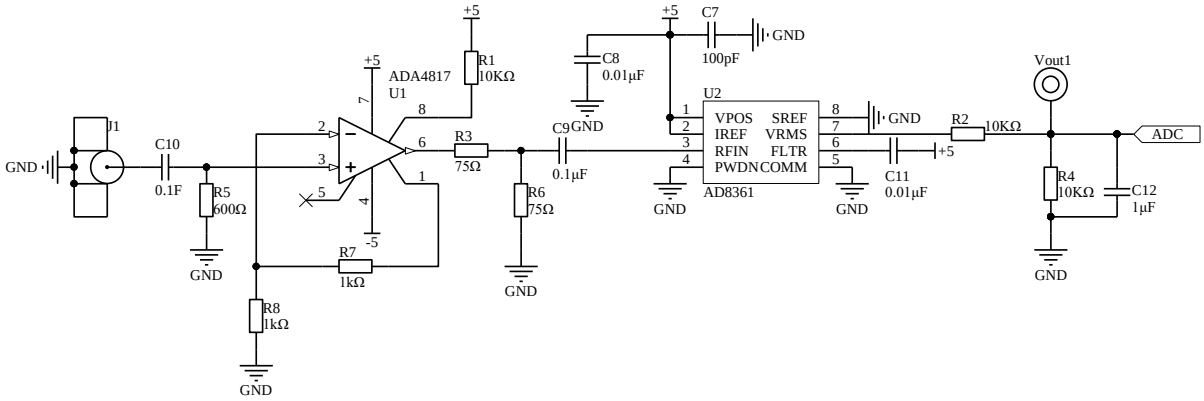

图 1　AD8361 检波器电路图

Figure 1　Circuit diagram of AD8361 geophone

2　延时电路模块

信号经过前期转换处理，高频信号发生器产生的模拟信号转化为数字信号，高频数字信号进行处理和分析采用 FPGA 实现，利用 FPGA 实现延时电路和信号频率测量电路，通过 SPI 通信协议与主控制器完成控制信号与数据的传递。

延时电路芯片采用 Cyclone2 系列，对信号调理电路所产生的方波信号进行延时，从而使得方波信号的输入输出之间产生时间间隔可调的时间差，从而达到对输入信号的延时作用[4][5]。FPGA 对数字信号处理的高速率确保延时时间的精准度和稳定性。延时程序[6]的核心思想：在时钟上升沿到来时，输入信号与后一信号进行逻辑与操作，从而完成对输入信号的延时，进而完成一次基准时钟频率的延时，基准时钟频率为 50MH z ，延时的步长为 20ns。达不到预期效果[7]。

调用芯片内部的模拟锁相环（PLL）对基准时钟的倍频，能够缩小延时的步进值[8][9]。经计算得知，如将基准频率倍频至 300MHz,延时的步进值过小，延时效率不高，占用逻辑门过多。倍频至 100MHz 又会导致时钟频率过低，无法满足测频电路所需要的时钟频率，测频的准确性不够高，因此倍频至 200MHz，延时的最小步长为 5ns，可以满足题设步长为 10ns 的要求。时钟频率可满足测频时钟要求，理论测频精度可达到题设要求。

延时时间利用四个外设按键来设定，即设定延时多少步长。程序对四个独立按键进行实时监测，判断按键是否被按下，从而确定输入的延时时间。为防止按键的误触和多次重复按下导致输入延时时间不正确，加入了按键去抖动程序，输入完成后按下确认键，以此来确保外部输入延时时间的准确性。

经实际测试，实际延时步长为 5ns，可以满足题目中的步长要求，利用外部按键输入延时时间的方法可行，并未出现按键时间读取错误，对 100Hz-20MHz 频段范围内的输入信号进行延时，均能达到预期效果。

3　频率测量模块

常见的测频方法有测周期测频、法定时计数法和等精度测频三种。测周期法常用于测量低频段信号频率，等精度测频所测频带范围宽，且高、低频段的测量精度一致[10]。

待测频率跨度为 100Hz-20MHz，步进值 10Hz，等精度测频[11]的方法进行测频相对复杂。经计算采用定时计数法测频率可以满要求，因此采用定时计数法测量输入信号频率。

FPGA 的基准频率为 50MHz，经锁相环 4 倍频为 200MHz，假设闸门时间为 1s，占用硬件资源过多，测频的实时性会受到影响。闸门时间过短又会导致测量低频段的±1 误差影响较大。经过实际测试，设置闸门时间为 0.5s 既能保证测量精度，削减±1 误差[12]带来的影响。

FPGA 测频后得到的数据为二进制数，无法显示出所得频率，在 FPGA 和主控制器之间采用 SPI 通信协议进行数据传送。主控制器（STM32）发送指令的同时 FPGA 把所获取的二进制数传送给主控制器[13]，主控制器通过解码和数学运算得出待测信号的频率。

经过实际测试，FPGA 与主控制器的通信正常，测频模块发送给主控制器的二进制数经过译码运算后，所得结果即为输入信号的频率。对比示波器所测得的频率，测频结果准确，实时行好，误差在允许范围内，能够满足题设要求。

4 测试方案与测试结果

4.1 测试方案

(1) 将装置链接并控制 DDS 的频率控制字和幅值控制字使其输出幅值在 10mV-200mV 之间、频率为 100Hz-20MHz 的任意正弦波，利用示波器检测装置的延时和测频性能。

(2) 通过对比测频模块及示波器验证测频模块的准确性。

(3) 通过对比设置的延时时间及示波器显示结果验证延时模块的准确性。

(4) 通过对比设置的幅值及示波器显示结果验证检波模块准确性。

4.2 测试结果

硬件电路搭建完毕后经测试，检波电路、延时器电路模块、频率测量模块均达到预期目标，各个电路模块的稳定性较高，可以满足设计要求。各个电路模块经级联调试后，测量各个频率范围内的检波模块的检波效果、延时电路延时时间间隔、频率测量电路测频数据如表 1、2、3 所示。

表 1 检波准确度检验

Table 1 Detection Accuracy Test

设置有效值（mV）	1KHz 输出幅度（mV）	1KHz 相对误差（%）	100KHz 输出幅度（mV）	100KHz 相对误差（%）	20MHz 输出幅度（mV）	20MHz 相对误差（%）
20	21.6	8.0	21.6	8.0	20.6	3
40	40.8	2.0	40.8	2.0	41.6	4
60	60.8	1.3	60.0	0.0	61.5	2.5
80	80.0	0.0	80.0	0.0	82.0	2.5
100	100.0	0.0	100.0	0.0	104.0	4

表 2 延时电路测试

Table 2 Delay Circuit Test

输入方波频率	设置延时	实测值	绝对误差
1KHz	100ns	95.000ns	5.000ns
1KHz	100us	99.993us	0.007us
100KHz	100ns	93.600ns	6.400ns
100KHz	100us	99.973 us	0.027us
20MHz	100ns	99.000ns	1.000ns
20MHz	100us	99.960us	0.040us

表 3　测频模块测试

Table 3　Frequency measurement module test

设置频率	输出频率	相对误差（%）
1 kHz	1.021kHz	2.1
10 kHz	10.00kHz	0
100 kHz	100.156kHz	0.16
1 MHz	999.031kHz	0.1
10 MHz	9.999MHz	0.1
20MHz	19.986MHz	0.1

5　结论

电路延时及频率测量装置经过实际测试得知，输出信号峰-峰值 8mV 时无明显失真，信号要求频带范围内无明显失真，可实现峰峰值小于 200mV、频率 1kHz-100kHz 的信号整形为方波，幅度为 3±0.5V。延时模块延时时间范围为 100ns-100ms，程控可调，调节步长小于 10ns。测量装置的分辨力为 0.1μs，绝对误差为 1μs，并能显示延时前后的波形。经实际测试，所设计的电路延时及频率测量装置达到题干要求。该设计获得 2018 年吉林省电子设计大赛二等奖。

参考文献

[1] 张英平,姬家好,李国军.基于单片机的简易电路延时测量装置研究与设计——学生实践训练成果[J].数字技术与应用,2018,36(12):129-130.

[2] 黄志文,卢美吉,钟绪杰,王春梅,韦善于.基于 FPGA 的数字频率测量装置设计[J].电子技术,2018,47(12):78-79+66.

[3] Alan V.Oppenheim， Alan S.Willsky， S.Hamid Nawab. Signals and Systems，Second Edition[M]. 北京：电子工业出版社，2009.6

[4] 康华光.电子技术基础·模拟部分（第六版）[M]. 北京：高等教育出版社，2006.1

[5] 林畅,庞辉,常彬,刘栋,翟雪冰,高路,闫鹤鸣.基于 FPGA 的直流断路器仿真建模与延时补偿算法[J].电网技术,2018,42(05):1417-1423.

[6] 凌佳俊,董颖辉.基于 FPGA 的信号延时器研究与设计[J].信息通信,2015(09):73-74.

[7] 马飞,刘琦,王鹏,郑先国.基于 FPGA 的信号微小延时方法[J].计算机测量与控制,2015,23(08):2868-2870+2874.

[8] 裴亮锋,陈自力.基于 FPGA 的延时块 LMS 均衡器的设计与实现[J].计算机测量与控制,2013,21(01):184-187.

[9] 王鹏翔,周灏,来金梅.基于数字延时锁相环的 FPGA IO 延时管理电路[J].复旦学报(自然科学版),2013,52(04):497-504.

[10] 王彦东,邵英,王黎明,肖雄波.基于 FPGA 的智能高精度频率测量设计[J].中国测试,2014,40(04):119-12.

[11] 徐德仁,黄明,王灿,吉祥.宽带等精度数字测频系统设计[J].电子科学技术,2016,03(06):685-688.

[12] 刘梅英.基于 FPGA 的频率测量计的设计与实现[J].电子技术与软件工程,2017(23):84-85.

[13] 潘宇.基于 FPGA 和 STM32 的脉宽频率测量方法[J].实验室研究与探索,2017,36(02):83-86.

基于室内稳定的多功能飞行系统设计*

张　越；郑卓然；刘鉴辉

（吉林大学 仪器科学与电气工程学院，　长春 130021）

摘要：随着现代社会科技不断进步，越来越多的研究者开始关注于空中机器人在室内环境下的自主飞行问题。由于室内无线信号屏蔽、干扰等的影响较为严重，基于 GPS 信号、无线定位信号等常用定位信号无法定位，因此会导致难以保证飞行器系统的稳定性。正因为上述原因，本设计采用多传感器的控制系统，依靠自带传感器，通过数据融合和处理实现对周围环境的感知，实现四旋翼飞行器的室内稳定飞行，其中包括固定高度飞行和固定点飞行。另外，本设计采用完全开源的飞行控制器和可自由更换的传感器，实现了飞行器系统的模块化，并且给以后的设计者以改进空间。

关键词：四旋翼飞行器　室内　稳定　多传感器　定高　定点

The design of multifunctional flight system based on indoor stability

Zhang yue；Zheng Zhuoran；Liu Jianhui

（Jilin University,College of Instrumentation &Electrical Engineering,Changchun 130021,China）

Abstract：With the continuous advancement of modern social science and technology, more and more researchers have begun to pay attention to the problem of autonomous flight of aerial robots in indoor environments. Due to the serious influence of indoor wireless signal shielding and interference, common positioning signals based on GPS signals and wireless positioning signals cannot be located, which makes it difficult to ensure the stability of the aircraft system. For the above reasons, the design uses a multi-sensor control system, relying on its own sensors, through data fusion and processing to achieve the perception of the surrounding environment, to achieve indoor stable flight of the four-rotor aircraft, including fixed altitude flight and fixed point flight. In addition, the design uses a completely open source flight controller and freely replaceable sensors to achieve modularization of the aircraft system and to improve space for future designers.

Key words：Four-rotor aircraft　Indoor　Stable　Multi-sensor　Altitude hold　Point hold

0　前言

四旋翼飞行器是一种高智能的自主飞行器，由于其在军事和民用领域具有较为广阔的应用前景，而四旋翼无人飞行器质量轻、载重小、续航能力差的特点决定该无人飞行器主要是在低空的近地面进行短航时工作，如室内、峡谷、树林等。近年来，众多科技爱好者和学者致力于四旋翼飞行器装置、导航和控制方法的研究[1]。随着地面移动机器人在未知环境中自主导航技术的发展越来越多的研究者开始关注于空中机器人在室内环境下的自主飞行问题。对于室外作业的飞行器而言，常采用惯性传感器与 GPS 数据相融合的方法实现飞行器状态的稳定与控制。但是由于在室内环境下无线信号屏蔽、干扰等的影响较为严重，基于 GPS 信号、无线定位信号等常用定位信号无法定位，目前就急需室内飞行的控制方法。

由此利用多传感器的控制系统便由此提出[2~4]，也带来了如下要求，感知性：依靠自带传感器，通过数据融合和处理实现对周围环境的感知；鲁棒性：由于温度、气流等扰动会对传感器数据造成干

* 指导老师：易晓峰

项目类型：大学生创新训练项目（2018B6528）

扰，系统需要克服这些扰动的影响等困难。

1 系统总体设计方案

基于室内稳定的多功能飞行器系统的总体设计思想，本设计由开源飞控，定高模块，定点模块三部分组成。其中飞控控制飞行器姿态，定高模块采用超声波传感器以获取当前飞行高，在垂直方向控制四旋翼飞行器；定点模块采用光流传感器以获取地面纹理信息，在水平方向控制四旋翼飞行器[5]。

最终此系统实现了飞行器一键起飞、一键降落、定高飞行、定点飞行，并且有拓展性，可以在此基础上进行功能添加。

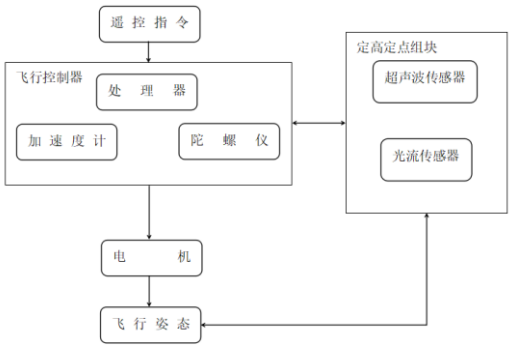

图 1 系统原理框图

Fig. 1 System block diagram.

2 四旋翼飞行器的组装与调试

四旋翼飞行器的框架模式分为 X 模式和十字模式。十字模式的前进方向与四轴中的一个电机致，也就是飞控板上的箭头指向其中一个电机，而在 X 模式下，飞控板上箭头指向的是前端两个电机的中间位置。相比较于 X 模式，十字模式能够清楚的区分机头与机尾，在飞行中十字模式的修正力较小比较容易控制。X 模式，依靠 3 轴姿态控制，4 个电机都需要进行调整，所以在飞行过程中修正力较大，但是相比于十字模式，X 模式更加灵活速度更快，也非常适合特技飞行。本文所讲飞行器将采用 X 模式。

本设计采用的是直流无刷电机。直流无刷电机由电动机主本和驱动器(电调)组成，是一种典型的机电体化产品。直流无刷电机(BLCD)既具备直流电动机运行效率高、无励磁损耗以及调速性能好的优势，又具有交流电动机的结构简单、运行可靠、维护方便等特点，已广泛应用于办公自动化设备、仪器仪表、计算机外围设备、医疗器械、家用电器和航空航海等领域。在四旋翼飞行器的电机驱动系统中，控制器完成的主要工作是实现电机的转速控制。当电机开环启动后，进入闭环工作状态，通常由控制器通过 PWM 控制 MOSFET 的导通和关断，进而达到调节电机的转速的目的。

实际上对于四旋翼飞行器，电机与螺旋桨的搭配是个非常复杂的问题，它牵扯到其自身产生的升力与飞行器自身的重量与姿态的平衡。当螺旋桨的尺寸越大，那么其产生的升力就越大，但是需要更强的驱动力。当螺旋桨的尺寸越小，其产生的升力就越小，那么其需要更高的转速以弥补其升力的不足。

四旋翼飞行器的动力部分是整个飞行器设计的核心，而对于电机的精准控制直接地决定了飞行器的稳定性，在调试过程中无人机在横滚，俯仰，油门，偏航任一输出的误差都会直接地影响到飞行器的姿态，我们采用的调试方法是单一变量法，先锁定除油门输出以外的其它输出，通过绳索简单控制飞行器在水平方向上的位移，结合实际的飞行姿态，对理论 PID 参数进行简单优化处理以实现飞行器在单一方向上的理想飞行，以此类推再解锁其他的通道输出，针对光流返回的灰度数据对水平面上的 X 轴和 Y 轴分别进行 PID 调节，以实现飞行器最终的自动稳定飞行[6]。

3 计算结果与比较

高度控制采用双闭环 PID 控制的方法。四旋翼正常飞行时，传感器突然遇到外界干扰，会造成传感器采集数据失真，解算出错误高度，只采用高度单闭环情况下，使系统很难稳定运行。因此，引入 z 轴加速度环作为内环，进行 PID 控制，可有效避免外界干扰造成的影响，增强了系统的鲁棒性。PID 的输出为油门值，油门给定电子调速器值，电子调速器控制电机使空间三轴欧拉角和高度变化。

$$AngelPIDout(t)=$$

$$k_p e(t)+k_i\sum_{j=0}^{t}e(j)T+k_d\left[e(t)-e(t-1)\right]/T \quad (1)$$

$$AngelRatePIDout(t)=$$

$$k_p' e'(t)+k_i'\sum_{j=0}^{t}e'(j)T+k_d'\left[e'(t)-e'(t-1)\right]/T \quad (2)$$

PID 控制算法采用位置式数字 PID 控制，式（1）为高度环 PID 公式，公式（2）为加速度环 PID 计算公式，AngelPIDout(t)为高度环 PID 输出，AcceleratePIDout(t)为加速度环 PID 输出。e(t)=期

望高度-实际高度，e′(t)=AltitudePIDout(t)-（z 轴加速度-重力加速度值）。

PID 输出值先经过限幅处理，再输出给油门，防止某些时刻输出油门值过大，造成过冲，使系统难以稳定。通过不断调节 K_p、K_i、K_d、$K_p^{'}$、$K_i^{'}$、$K_d^{'}$ 六个参数并在四旋翼飞行器上进行测试，最终得出能让飞行器定高稳定飞行的一组值。高度 PID 控制总体流程如图 2 所示[7~10]。

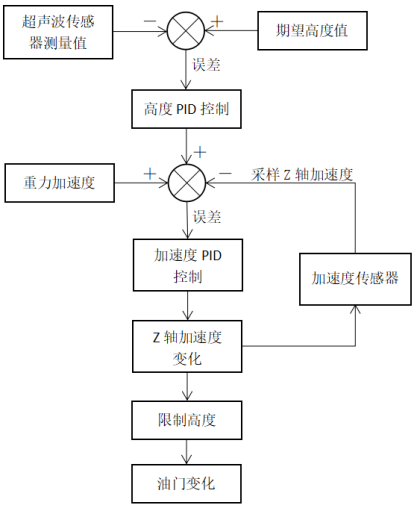

图 2　高度 PID 总体流程图

Figure 2　High PID overall flow chart

4　定点功能实现

进行水平面内的位置环和速度环的串级 PID 控制。所谓串级控制，就是采用两个控制器串联工作，外环控制器的输出作为内环控制器的设定值，由内环控制器的输出去操纵控制阀，从而对外环被控量具有更好的控制效果。本设计采用位置环与速度环对飞行器进行水平方向的控制。

首先需要对光流数据进行处理，第 1 步，对积分位移进行一个简单的低通滤波。第 2 步，用姿态角去补偿积分位移。第 3 步，对积分位移进行微分处理，得到速度。第 4 步，把数据单位转换为厘米。至此，光流数据的处理算是基本完成了，有了积分位移和微分速度这两个参数，就可以进行水平面内的位置环和速度环的串级 PID 控制了。

光流控制中外环进行位置控制计算目标速度给内环，内环进行速度控制，计算目标角度，调试先调速度环然后调试位置环，最后进行补偿，即对上述积分位移进行角度补偿，得到不受姿态影响的位置，至此定点功能实现[11~13]。

5　四旋翼飞行测试

根据 IHS Markit-份最近的研究显示，在没有额外负载的理想条件下飞行，市场上近 50%无人机的预期电池续航时间不足 30 分钟,35%无人机的飞行时间为 31~60 分钟其余 15%和更少的无人机的飞行时间能超过 1 小时。Ihs Markit 数据传输和管理服务高级分析师 Stelios Kotakis 表示:“飞行时间一直是娱乐型四轴飞行器和专业无人机在设计方面所面临的最大挑战，尤其对于那些被公司用于超视距操作的飞行器而言更是如此。快递公司希望无人机具有更长的电池续航时间，并且正在进行无人机运送包裹的测试，以确定无人机的使用效果。”

因而，飞行器的续航时间与对本项目所设计的室内稳定飞行器系统至关重要。对此设计的飞行器进行续航测试：

表 1　飞行器续航测试

Table I　Endurance test of the aircraft

空载载重 2.11kg

	总重量	起始电池电压	持续时间△h≤h*10%
测试 1	2.11kg	12.4V	6min24s
测试 2	2.11kg	12.4V	6min20s
测试 3	2.11kg	12.4V	6min20s

增加载重至 2.40kg

	总重量	起始电池电压	持续时间△h≤h*10%
测试 1	2.40kg	12.4V	6min02s
测试 2	2.40kg	12.4V	6min05s
测试 3	2.40kg	12.4V	6min07s

增加载重至 2.80kg

	总重量	起始电池电压	持续时间△h≤h*10%
测试 1	2.80kg	12.4V	5min20s
测试 2	2.80kg	12.4V	5min27s
测试 3	2.80kg	12.4V	5min22s

在此设计中，基本满足飞行要求。如需增加飞行时间，可以减少载重量或增大电池容量。

6　总结与展望

现有无人机在室内飞行多为手动控制，十分依赖于操作者的技术水平。

本设计采用开源飞行控制器，搭建了基于超声笔传感器的定高飞行模块，和基于光流传感器的定点模块，多传感器融合，可以在 GPS 信号、无线定位信号等常用定位信号无法有效使用时——即室内飞行，对飞行器进行精准的控制，实现定点定高寻迹避障等功能。至此，不仅保证了飞机的稳定，更降低了对操纵者的水平要求，实现自动控制，也更可以面向广大消费者而不是特殊群体，实现飞行器的普及化。

本设计中，满足了室内环境下的定高定点飞行的需求。有望应用于室内航拍、室内搜救、室内监控、室内巡逻、短距离投递和飞行器操控训练等处。

望后继者可以对定高定点模式进行优化，使其更加稳定可靠，或增加避障等功能。

参考文献

[1] 肖支才,姜鹏,戴洪德,康宇航. 室内四旋翼无人飞行器定位导航的研究现状与关键技术[J]. 飞航导弹,2014,(08):25-29.

[2] Fei WANG,Jin-Qiang CUI,Ben-Mei CHEN,Tong HLEE. A Comprehensive UAV Indoor Navigation System Based on Vision Optical Flow and Laser FastSLAM[J]. Acta Automatica Sinica,2013,39(11):.

[3] B. C. Min,C. H. Cho,K. M. Choi,D. H. Kim. Development of a Micro Quad-Rotor UAV for Monitoringan Indoor Environment[M].Springer Berlin Heidelberg:2009-06-15.

[4] 李帅阳,武凌羽,张长毛,马忠丽. 基于多传感器的微型四旋翼室内自主悬停研究 [J/OL].:1-6(2017-03-27).

[5] 马斯, 周天鸿, 刘福彬, et al. 四旋翼飞行器自旋稳定与定高稳定飞行的实现[J]. 数字通信世界, 2015(12).

[6] 吕品,赖际舟,杨天雨,刘建业,朱斌,宋亦凡. 基于气动模型辅助的四旋翼飞行器室内自主导航方法[J]. 航空学报,2015,36(04):1275-1284

[7] 陈小龙,唐强,车军,刘林. 基于人工视觉的四旋翼飞行器室内定位与控制[J]. 兵工自动化,2012,31(05):61-64.

[8] 于拓. 面向四旋翼飞行器的室内定位系统[D].上海交通大学,2015.

[9] 张毓斐,沈兴鑫. 基于 STM32 的未知室内能自主避障飞行四旋翼空中机器人系统总体设计[J]. 科技传播,2016,8(02):184-185.

[10] 魏青铜. 室内环境下基于 SLAM 的四旋翼无人机定位与控制[D].南京航空航天大学,2016.

[11] 郝伟. 基于任务的四旋翼飞机室内自适应导航方法研究[D].中国民航大学,2014.

[12] 窦慧洋. 无人机室内避障、巡航与热源跟踪的设计与实现[D].内蒙古大学,2017.

[13] 马斯, 周天鸿, 刘福彬, et al. 四旋翼飞行器自旋稳定与定高稳定飞行的实现[J]. 数字通信世界, 2015(12).

基于手机监控的充电控制装置的设计*

陈依涵；向梦航；吴　铮

（吉林大学 仪器科学与电气工程学院　长春 130021）

摘要：现代社会科技不断进步，电子数码类产品发展很快。人们对手机、笔记本电脑、智能穿戴设备等便携式电子产品的依赖性逐渐增强[1]。性能好配置高的设备为人们工作生活提供便利的同时，其充电过程中的问题也暴露出来。本装置通过添加监测充电数据的模块，使用户可以从充电显示屏或者远程上实时了解充电状况。本装置机身加设环境数据检测电路，将充电过程的温度、湿度等环境状况远程反馈给用户，方便用户掌握设备周围的充电环境[2-5]。

关键词：充电　监控　环境

The design of charging control device based on mobile phone monitoring

Chen Yihan；Xiang Menghang；Wu Zheng

（Jilin University,College of Instrumentation &Electrical Engineering,Changchun 130021,China）

Abstract：The modern society has made continuous progress in science and technology, and electronic digital products have developed rapidly. People's dependence on portable electronic products such as mobile phones, laptops, and smart wearable devices has gradually increased[1]. While the equipment with high performance and high configuration provides convenience for people's work and life, the problems in the charging process are also exposed. The device adds a module for monitoring the charging data so that the user can know the charging status in real time from the charging display or remotely. The device body is provided with an environmental data detecting circuit to remotely feedback the environmental conditions such as temperature and humidity of the charging process to the user, so that the user can grasp the charging environment around the device[2-5].

Key words：Charging　Monitor　Environment

0　前言

基于手机监控的充电控制装置的设计主要针对平板电脑和苹果 Mac 等轻薄商务笔记本为例进行研究设计[6-7],由硬件系统（多用磁吸电源线\直流电压电流可调电路，充电数据收集模块\Wi-Fi 模块）和软件系统（手机端软件应用）构成。

本设备采用“互联网＋”的软硬件相结合的模式，通过硬件采集数据，本地收集处理数据，终端智能软件显示，实现线上线下的紧密联系[8-10]。

1　系统设计方案

基于手机监控的充电装置的的设计思想：本设计由 STM32F103C8T6 单片机核心板控制，整个电路由充电电路，控制电路，监测电路，LCD 显示电路以及蓝牙模块电路 5 个部分构成的。其中监测电路包括电压，电流监测电路以及温湿度的监测电路。

2　充电电路设计

本设计首先经过直流电源通过 XL6009 升压模块实现 5V~35V 电压的输出范围，为设备进行充电。通过单片机的控制信号实现对设备的过充保护和电流控制[11]。

XL6009 升压模块电路原理图如图 1 所示。其主要由 XL6009 升压型直流电源变换器芯片、二极管以及电感电容等构成。

* 指导老师：王永志

项目类型：大学生创新训练项目（2018B6554）

其中，XL6009 的升压型直流电源变换器芯片的 3 管脚作为方波输出信号。

当 3 管脚输出显示为低电平时，由于二极管的单向导通性，D1 截止，电感 L1 作为一个储能元件储存电压，而此时电容 C1 与和 R1 组成一个回路放电，使输出电压下降；当 3 管脚输出显示为高电平时，同理，D1 此时导通，电感 L1 向电容两端充电，输出电压升高。

R1 和 R2 是 XL6009 芯片内部组成的电压放大器，通过负反馈使输出电压稳定，可以由电阻 R1 和 R2 控制其电压的放大倍数[12]。

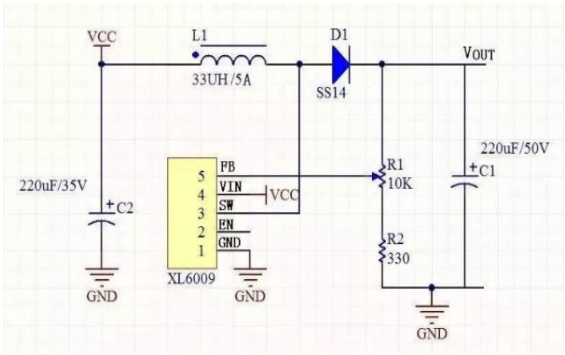

图 1　升压模块电路原理图

Fig.1　Circuit schematic diagram of boost module

3　监测电路设计

为保证整体充电过程的设备的安全，因此，必须实时监测充电过程的重要参数。

其中电压、电流和功率是最基本的三个测量指标。此外考虑到充电环境的复杂性和智能设备的适应性，本装置还加入了温度及湿度。

电流、电压和功率等数据被采集处理后实时显示在装置上。通过采用温湿度传感器，ACS712 电流检测模块等实现对充电电路实时监测[13]。

如图 2 所示。

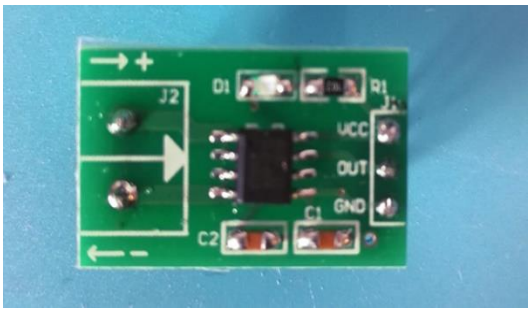

图 2　ACS712 电流检测模块

Fig.2　ACS712 Current Detection Module

为验证其功能，我们找寻了市面上常见的手机型号的锂电池进行了电压、电流的测试，实测数据如表 1 所示。

表 1　电压电流功率数据

Table 1　Voltage and Current Power Data

电压(v)	4.1	4.1	4.1	4.1	4.1	4.1	4.1
电流(I)	0	0	0	0	0	0	0
电压(v)	4.1	4.1	4.1	4.1	4.1	4.1	4.1
电流(I)	0	0	0	0	0	0	0
电压(v)	4.2	4.2	4.2	4.2	4.2	4.2	4.2
电流(I)	0	0	0.17	0.16	0.12	0.15	0.15

此外，我们也用温度计比较了实测温度与传感器示数，数据对比图如图 3 所示。

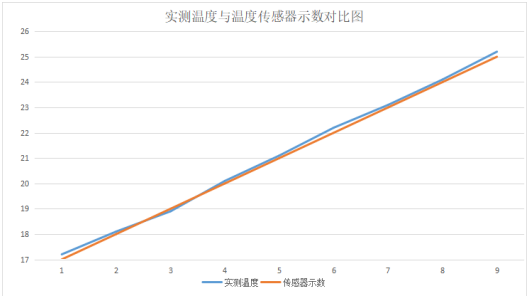

图 3　实测温度与传感器示数对比图

Fig.3　Contrast Diagram between Measured Temperature and Sensor Indicators

最后，利用湿度计检验实测湿度与传感器示数，数据对比图如图 4 所示。

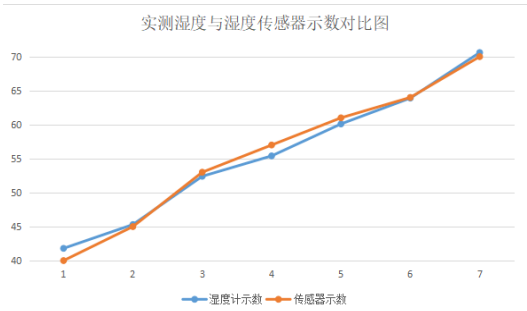

图 4　实测湿度与传感器示数数据对比图

Fig.4　Contrast Diagram between Measured Humidity and Sensor Indicator Data

4　显示电路设计

数据采集显示电路包括数据采集端 LCD 显示系统和移动显示端两个部分。LCD 显示直接通过单片机进行控制输出显示。移动端通过蓝牙模块和手机设备进行通信，在 app 上实时显示各种数据[14-15]。

5　结论

本文设计了一种基于手机监控的充电装置，通过传感器采集的数据进行实时显示与传输，使使用者清楚地知道当前充电的状态，为设备充电提供了

一定的保障。

参考文献

[1] 沙占友, 庞志锋, 张苏英. 手机电池恒流/恒功率充电器的电路设计[J]. 电测与仪表, 2001, 38(5): 31-33.

[2] 刘美俊. 基于单片机的通用智能充电器设计[J]. 仪表技术与传感器, 2006,9: 41-43.63.

[3] 方平, 周繁华. 简易万能充电器的设计[J]. 电子制作, 2013,8X: 6-6.

[4] 何立民. 单片机应用技术选编 1/2/3[M]. 北京：北京航空航天大学出版社，1992.

[5] 谢筑森. 单片机开发与典型应用设计[M].北京：机械工业出版社：1997 年 9.

[6] Bodson D. One-Size-Fits-All Mobile Phone Charger [Standards][J]. IEEE Vehicular Technology Magazine, 2011, 6(3): 107-110.

[7] Qu A D, Zhang Z H. The Design of Charger based on 1T SCM[C]//Applied Mechanics and Materials. Trans Tech Publications, 2013, 347: 1553-1556.

[8] Kim C G, Seo D H, You J S, et al. Design of a contactless battery charger for cellular phone[J]. IEEE Transactions on Industrial Electronics, 2001, 48(6): 1238-1247.

[9] Ziadi Y, Qjidaa H. A High Efficiency Li-Ion Battery LDO-Based Charger for Portable Application[J]. Active and Passive Electronic Components, 2015, 2015.

[10] Li X Z, Hu G M, Hou P X, et al. Analysis on Harmonics Caused by Connecting Electric Vehicle Chargers with Power Network[C]//Advanced Materials Research. Trans Tech Publications, 2013, 724: 1393-1397.

[11] 刘宴兵,刘飞飞.基于云计算的智能手机社交认证系统[J] .通信学报, 2017,33(Z1): 28-34.

[12] 卢文科编著 实用电子测量技术及其电路精解[M].北京：国防工业出版社，2000.

[13] (美)D.H.施因果德编著，徐德炳译 传感器的接口及信号调理电路[M].北京：国防工业出版社，1984.1

[14] 杨兴强, 孙国良. 一种基于单片机的手机电池智能充电系统[J]. 南阳师范学院学报, 2009, 8(12).

[15] 张海望,杨波.云计算在手机通信中的应用研究[J]. 计算机安全,2011: 49-51.

第二部分　英文论文集

PART II　ENGLISH PROCEEDINGS

Research on Intelligent Car Based on Raspberry Pi and UWB Technology

SHANG Hujun；WANG Zhiying；LI Zhixin

（Jilin University,College of Instrumentation &Electrical Engineering,Changchun 130021,China）

***Abstract*—With the development of industrial automation and the increasing demand for location-based services, positioning and navigation technology has entered an era of rapid development. Using wireless communication technology for indoor positioning has become a hotspot of navigation technology research. In this paper, the indoor positioning, wireless video transmission and obstacle avoidance technology of the car were studied. An indoor UWB wireless positioning system composed of one tag and three base stations is constructed, and the location is realized by TOF method. The multi-sensor obstacle avoidance technology and algorithm based on the combination of ultrasonic and infrared are studied. In the aspect of obstacle avoidance algorithm, the direction of obstacle avoidance is determined by the position relationship between obstacle and car. Video transmission between raspberry pie and host computer is realized by means of WIFI communication technology. The upper computer software is developed to display the car position coordinates and the transmitted video.**

***Key words*—Navigation technology Video transmission UWB positioning Multi-sensor obstacle avoidance**

I. PREFACE

WITH the establishment of large shopping malls, factories and other large venues, the demand for indoor positioning and navigation is increasingly strong. This paper USES UWB indoor positioning technology, first through TOF algorithm ranging, and then through three-sided positioning algorithm to achieve the indoor positioning of intelligent car [1-3].A multi-sensor hardware obstacle avoidance platform combining ultrasonic and infrared was built, and the wireless video transmission between the on-board camera and the terminal was used to monitor the environment information around the car in real time.The car can avoid obstacles independently in the process of driving, and the operator can monitor the real-time position of the car and the surrounding environment in the upper computer interface.

II. OVERALL DESIGN SCHEME

The research content of this design includes UWB positioning principle, software and hardware design of obstacle avoidance system WIFI communication and upper computer display.

The overall design scheme is shown in figure1.

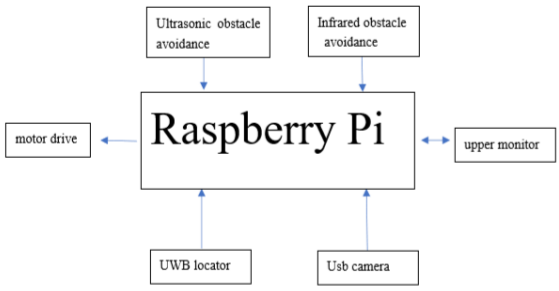

Figure 1 Overall scheme design

The design needs to achieve the following goals:

(1) transmit the video captured by the on-board camera to the host computer in real time with WIFI and display it;

(2) adopt UWB positioning to display the real-time coordinates of the position of the car on the upper computer;

(3) the car can use ultrasonic combined with infrared sensor obstacle avoidance module to avoid obstacles autonomously.

III. KEY TECHNOLOGIES AND DIFFICULTIES OF SYSTEM IMPLEMENTATION

A. indoor positioning of UWB

UWB (Ultra Wideband) is a carrier-free communication technology that USES narrow pulses of non-sinusoidal waves from nanoseconds to nanoseconds to transmit data.By transmitting

extremely low-power signals over a wide spectrum, UWB can achieve data transmission rates ranging from hundreds of mbits /s to several gbits /s in a range of about 10 meters.Compared with the traditional narrow-band system, the super-bandwidth system has the advantages of strong penetrating force, low power consumption, good anti-multipath effect, high security, low system complexity and high precision positioning.Therefore, hyper-bandwidth technology can be applied to indoor positioning and navigation of stationary or moving objects and people, and can provide very accurate positioning accuracy [4].

UWB positioning algorithm mainly consists of two parts. Firstly, TOF ranging algorithm is adopted to obtain the distance between the tag and the fixed base station, and then label coordinates are obtained according to the three-sided positioning algorithm.

(1) TOF ranging

DWM1000 ultra-wideband ranging, using the TOF (time of fly) ranging method, which is to calculate the radio electromagnetic wave transmission time, through the transmission time converted to distance.There are two devices, namely two DWM1000 modules, namely base station and label.The tag sends a message to the base station at the time of tA, which travels through the air for a time t1 and reaches the base station at the time of tB.After receiving the tag information, the base station will send the reply information to the tag at time tC after a period of time t2, and the message will be received at time tD after a period of time t1.As shown in figure 2:

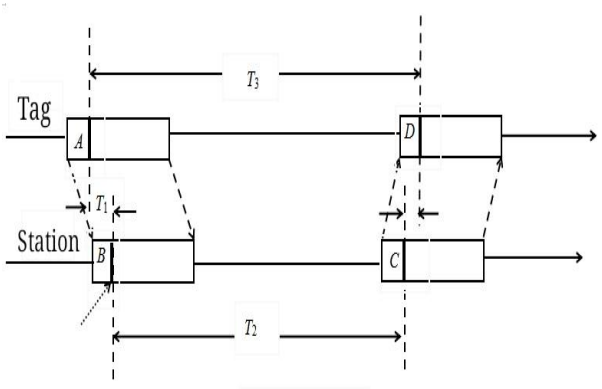

Figure.2 TOF ranging principle

The tag reads the register to get tA time and tD time stamps

$$t_3=t_D-t_A;$$

From the figure above we can see that there is another time t2, which is actually calculated in the label.The information sent to the tag by the base station includes the time stamp at the time of receiving the information B and the time stamp at the time of sending the information C. When the tag receives the information, t2 can be obtained by subtracting the two

$$t_2=t_C-t_B;$$

Different device clock frequency is the same, so two wireless signal transmission time

$$t=t_3-t_2;$$

The distance between the base station and the tag is

$$d=v*t/2$$

(2) Three-sided positioning algorithm

The distance between the tag and three base stations has been measured by TOF ranging, and the two-dimensional coordinates of the tag can be calculated by using the three-sided positioning algorithm based on these multiple distances.

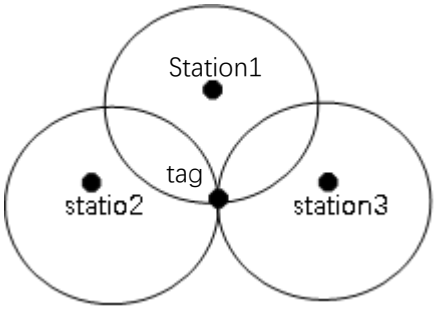

Figure.3 Principle of trilateral positioning

Suppose that the physical coordinates of the three base stations are (x1,y1), (x2,y2) and (x3,y3), the unknown tag coordinates are (x,y), and the ranging distance from the tag to the base station is d1,d2,d3, then there is a system of equations

$$(x-x_1)\text{^}2+(y-y_1)\text{^}2=d_1\text{^}2$$
$$(x-x_2)\text{^}2+(y-y_2)\text{^}2=d_2\text{^}2$$
$$(x-x_3)\text{^}2+(y-y_3)\text{^}2=d_3\text{^}2$$

The above equations are nonlinear equations. After subtracting the NTH equation from the first n-1 equation in the equations, the linearized equation can be obtained:

$$AX=b$$

Among them:

$$A=\begin{bmatrix}2(x_1-x_3) & 2(y_1-y_3)\\ 2(x_2-x_3) & 2(y_2-y_3)\end{bmatrix}$$

$$b=\begin{bmatrix}x_1\text{^}2-x_3\text{^}2+y_1\text{^}2-y_3\text{^}2+d_3\text{^}2-d_1\text{^}2 & 2(x_1-x_3) & 2(y_1-y_3)\\ x_2\text{^}2-x_3\text{^}2+y_2\text{^}2-y_3\text{^}2+d_3\text{^}2-d_1\text{^}2 & 2(x_2-x_3) & 2(y_2-y_3)\end{bmatrix}$$

We solved it using the least square method

$$X = (A^T A)^{-1} A^T b$$

B． Ultrasonic combined with infrared obstacle avoidance design

This design adopts ultrasonic obstacle avoidance module as the main obstacle avoidance part. As ultrasonic ranging has a blind area of 0-2cm, infrared switch module is added to assist obstacle avoidance.Ultrasonic ranging USES hc-sr04 ranging module, which can provide non-contact distance sensing function of 2cm-400cm, and ranging accuracy can reach 3mm.

Use detection round trip time to determine the distance between the car and the obstacle, the principle is to collect the ultrasonic wave from the ultrasonic transmitter, after the reflection of the obstacle, to the receiver to receive the ultrasonic wave used time is round trip time.The round-trip time divided by 2 and multiplied by the speed of ultrasonic wave propagation in the air is the distance between the car and the obstacle [5-6].

Under the rotation of the steering engine, the ultrasonic ranging sensor circulates to detect the distance of obstacles in the front, left and right directions, and the car judges the travel path based on the distance from obstacles in the three directions and the feedback from the infrared probe, so that the car can avoid obstacles autonomously [7].The obstacle avoidance algorithm combining ultrasonic ranging and infrared sensor is designed, and the algorithm flow chart is shown in figure 4.In the process of traveling, firstly, ultrasonic wave is used to detect the distance of obstacles in front. If the distance is greater than 30cm, continue to drive forward. Infrared assisted obstacle avoidance detection is used to avoid obstacles that may appear in the blind area of ultrasonic ranging.If the distance from the front obstacle is less than 15cm, it will go back. If the distance is between this distance, the steering gear will rotate to detect the obstacle distance on the left and right side of the car.If the distance between the left and right sides is less than 15cm, the car will move back.Otherwise, if the distance to the right is greater than the distance to the left, the car will turn right, and vice versa.

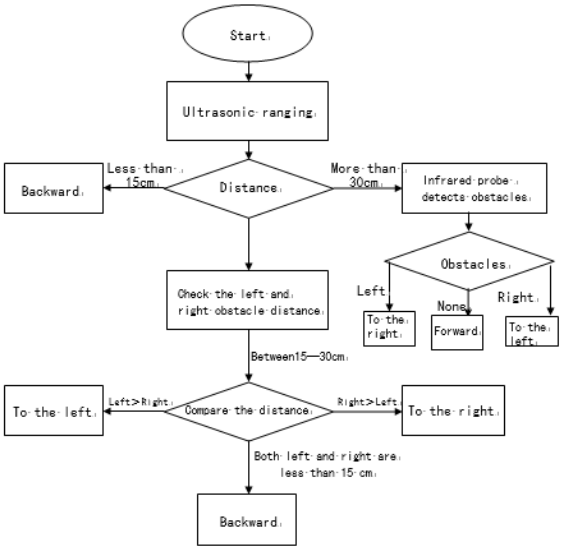

Figure.4 Flow chart of obstacle avoidance

Difficulties of ultrasonic obstacle avoidance technology: due to the characteristics of its own obstacle avoidance technology, it cannot guarantee normal operation in all kinds of scenarios, which requires constant experiments, trial and error, and continuous optimization algorithm to ensure normal operation in all kinds of scenarios without giving wrong instructions [8].

C． Remote video monitoring function

This function USES mjpg-streamer, an open source software supporting Linux system, as video monitoring software. It USES USB camera to collect video images of the surrounding environment of the car, and communicates with PC through WIFI network to realize real-time wireless monitoring of the surrounding environment [9].

Mjpg-streamer is a video streaming server based on IP address, using memory mapping [10].Through the analysis of terminal command, by the input plug-in input_uvc.So decomparts video shot in linux-uvc V4L2 device into independent jpeg image data and puts it into memory;The video data is processed by multiple output plug-ins;By the output plug-in output_http.So is responsible for taking video data out of memory and transferring it to the web page for display.

3 SYSTEM TEST RESULTS

A． overall vehicle structure

The overall physical picture of the intelligent car based on raspberry PI controller is shown in figure

5.The intelligent car consists of power supply system, control system, drive system, positioning system, autonomous obstacle avoidance system and video transmission system.

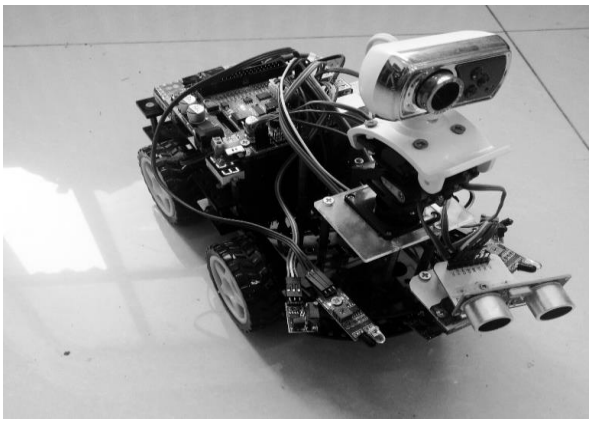

Figure.5 Top view of the car

B. system test

The final functions of the intelligent car based on raspberry PI controller are: self-positioning and display of position coordinates, wireless video transmission to the terminal, and use of ultrasonic combined with infrared sensor to achieve autonomous obstacle avoidance.The main test contents are as follows:

(1) independent positioning test. Open the coordinate display interface at the terminal to display the position coordinates of the label (car) in the coordinate system established with the main base station as the origin, as shown in FIG. 7;The positioning test results are shown in table 1 below.

Table 1 test results of UWB positioning system

Position number	Actual coordinates (cm)	Mean measured coordinates (cm)	Distance error (cm)
1	(60,60)	(65,67)	8.54
2	(60,120)	(66,108)	13.42
3	(120,120)	(127,110)	12.21
4	(180,120)	(182,107)	13.15
5	(180,180)	(190,168)	15.62
6	(240,240)	(238,252)	12.16

(2) video transmission test. Open the display interface of video on the upper computer, and you can see the real-time video shot by the on-board camera. Video is clear and smooth in the driving process of the car, and the display delay of video measured by a desktop timer is about 0.38 seconds.See figure 6.

Figure.6 Video delay testing

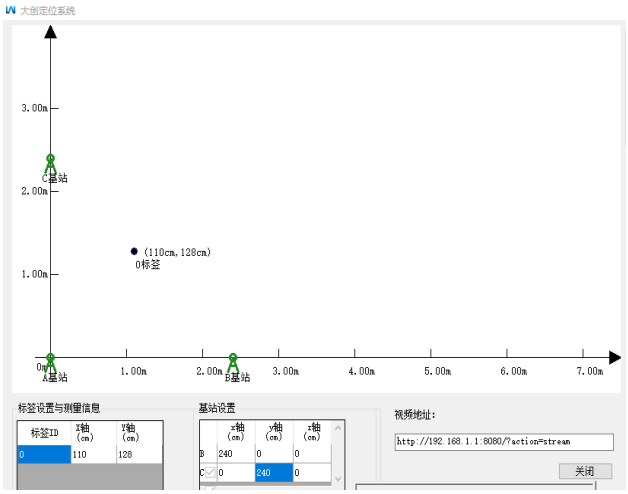

Figure.7 Coordinate display interface

(3) Autonomous obstacle avoidance test: put the car on a plane with certain obstacles. When the car encounters obstacles in the driving process, it can brake safely and continue to drive according to the relative position with obstacles. It can be seen that the autonomous obstacle avoidance function of the car is normal.

4 CONCLUSION

In this paper, an intelligent vehicle system based on raspberry PI controller is designed, and the TOF ranging method and principle, tri-edge positioning algorithm and its solution, ultrasonic obstacle avoidance principle and wireless video transmission scheme are introduced in detail.Through continuous debugging, all functions of the preset target of the car are basically achieved, and the coordinates of the car can be displayed in real time. The environment around the car can be monitored in real time through video transmission function, and video is clear and smooth,

so that obstacles in the direction of the car can be avoided autonomously.

References

[1] Li long wei, Hu Haiyan, Zhang Renhui, Li Chunguang, Sun Lining. Research on welcome robot system based on UWB indoor positioning [J]. Machinery and Electronics, 2018, 36 (12): 58: 63 68.

[2] Fan Ye, Chen Qiuxia, Ni Lihui. UWB robot indoor positioning system based on DWM 1000 module [J]. Single Chip Microcomputer and embedded system Application, 2018, 18 (11): 48 x 50 54.

[3] Zeng Guiling, Wang Ping, Zhang Yuming, Duan win glory. Intelligent handling car based on UWB [J]. Journal of Hubei Institute for nationalities (Natural Science Edition), 2019, 37 (02): 223.

[4] Li Wei, Ye Yan, Xie Jinxiong, Liu Taijun. UWB High Precision Indoor Positioning system and its implementation [J]. Data Communication, 2018 (05): 13 / 18.

[5] Ma duo, Dang Xiaojuan, Zhang Hui. Design and implementation of Ultrasonic Intelligent obstacle avoidance car [J]. Enterprise Science and Technology and Development, 2018 (09): 87 / 88.

[6] Xing Qiang, Yu Kathy, Gu Yuzhi. Distance balance obstacle avoidance strategy based on ranging ultrasonic sensor [J]. Modern Electronic Technology, 2018, 4 (20): 97 - 99 103.

[7] Wu Baotao, Kong Jinping, Wang Xiang. Design and implementation of intelligent car based on Arduino and raspberry pie [J]. Electronic Design Engineering, 2017, 25 (15): 58 / 61.

[8] Li Wenwen. Research on Barrier Avoidance of Automatic Navigation Trolley Based on Various Sensors[D]. Xi'an University of Science and Technology, 2008.

[9] Liu Hongbo, Zheng Shaowei, Xie Yuxi, Wang Jinjiang, Tang Qin. Design and implementation of embedded Wireless Video car [J]. Value Engineering, 2017, 36 (28): 138 - 139.

[10] He Zhichao, Kong Jinming, Wei Haute. Design of mobile monitoring car based on raspberry pie [J]. Science and Technology Plaza, 2017 (12): 78 / 80.

Design of multi-functional flight system based on indoor stability

Jianhui Liu；Yue Zhang；Zhuoran Zheng
（*Jilin University,College of Instrumentation &Electrical Engineering,Changchun 130021,China*）

***Abstract*—With the continuous advancement of modern social science and technology, more and more researchers have begun to pay attention to the problem of autonomous flight of aerial robots in indoor environments. Due to the serious influence of indoor wireless signal shielding and interference, common positioning signals based on GPS signals and wireless positioning signals cannot be located, which makes it difficult to ensure the stability of the aircraft system. For the above reasons, the design uses a multi-sensor control system, relying on its own sensors, through data fusion and processing to achieve the perception of the surrounding environment, to achieve indoor stable flight of the four-rotor aircraft, including fixed altitude flight and fixed point flight. In addition, the design uses a completely open source flight controller and freely replaceable sensors to achieve modularization of the aircraft system and to improve space for future designers.**

***Key words*—Four-rotor aircraft Indoor Stable Multi-sensor Altitude hold Point hold**

I. INTRODUCTION

THE four-rotor aircraft is a highly intelligent autonomous aircraft. Because of its broad application prospects in military and civilian fields, the characteristics of light weight, small load capacity and poor endurance of the four-rotor unmanned aerial vehicle determine that the unmanned aerial vehicle is mainly Short-season work at low altitudes, such as indoors, canyons, and woods. In recent years, many technology enthusiasts and scholars have devoted themselves to the research of four-rotor aircraft installation, navigation and control methods[1]. With the development of autonomous navigation technology for ground mobile robots in an unknown environment, more and more researchers have begun to pay attention to the problem of autonomous flight of aerial robots in indoor environments. For outdoor aircraft, the inertia sensor and GPS data are often used to achieve the stability and control of the aircraft state. However, due to the serious influence of wireless signal shielding and interference in indoor environments, common positioning signals based on GPS signals and wireless positioning signals cannot be located, and the indoor flight control method is urgently needed.

Therefore, the control system using the multi-sensor has also brought about the following requirements: Perceptuality: relying on the self-contained sensor to realize the perception of the surrounding environment through data fusion and processing; robustness: due to disturbances such as temperature and airflow To interfere with sensor data, the system needs to overcome the effects of these disturbances.

II. SYSTEM OVERALL DESIGN

Based on the overall design idea of the indoor stable multi-function aircraft system[2-4], the design consists of three parts: open source flight control, fixed height module and fixed point module. The flight control controls the attitude of the aircraft. The altitude module uses the ultrasonic sensor to obtain the current flight altitude, and controls the quadrotor in the vertical direction. The fixed point module uses the optical flow sensor to obtain the ground texture information and controls the quadrotor in the horizontal direction[5].

In the end, the system realizes one-button take-off, one-button landing, fixed-height flight, fixed-point flight, and expandability, and can be added on this basis.

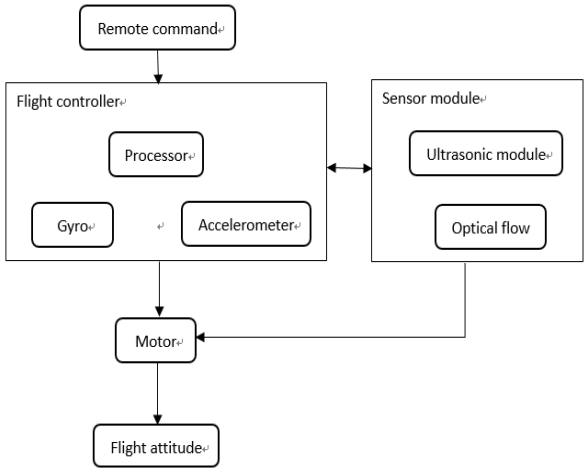

Fig. 1 System block diagram.

III. ASSEMBLY AND COMMISSIONING OF QUADROTOR

The frame mode of the quadrotor is divided into an X mode and a cross mode. The forward direction of the cross mode is caused by one of the four axes, that is, the arrow on the flight control board points to one of the motors, and in the X mode, the arrow on the flight control board points to the middle of the front two motors. Compared with the X mode, the cross mode can clearly distinguish the nose and the tail, and the correction force of the cross mode in flight is relatively easy to control. The X mode relies on 3-axis attitude control, and all four motors need to be adjusted, so the correction force is large during flight, but the X mode is more flexible and faster than the cross mode, and is also very suitable for aerobatics. The aircraft described in this article will adopt the X mode.

This design uses a DC brushless motor. The brushless DC motor consists of the motor main and the driver (electrical adjustment), which is a typical electromechanical product. Brushless DC motor (BLCD) not only has the advantages of high operating efficiency, no excitation loss and good speed regulation performance of DC motor, but also has the characteristics of simple structure, reliable operation and convenient maintenance of AC motor. It has been widely used in office automation equipment. Instruments, computer peripherals, medical equipment, household appliances and aviation and navigation. In the motor drive system of a four-rotor aircraft, the main work done by the controller is to achieve the speed control of the motor. When the motor is opened, it enters the closed-loop working state. Usually, the controller controls the turn-on and turn-off of the MOSFET through PWM, thereby achieving the purpose of adjusting the rotational speed of the motor.

In fact, for a four-rotor aircraft, the combination of the motor and the propeller is a very complicated problem, which involves the balance between its own lift and the weight and posture of the aircraft itself. When the size of the propeller is larger, the lift generated by it is greater, but a stronger driving force is required. The smaller the size of the propeller, the less lift it produces, and it requires a higher rotational speed to compensate for its lack of lift.

The power part of the quadrotor is the core of the entire aircraft design, and the precise control of the motor directly determines the stability of the aircraft. During the commissioning process, the error of any output of the drone, roll, pitch, throttle and yaw during the commissioning process It will directly affect the attitude of the aircraft. The debugging method we adopt is a single variable method, which first locks the output other than the throttle output, and simply controls the displacement of the aircraft in the horizontal direction through the rope, combined with the actual flight attitude, the theoretical PID. The parameters are simply optimized to achieve the ideal flight of the aircraft in a single direction, and so on to unlock other channel outputs, and the gray-scale data returned by the optical flow is PID-adjusted to the X-axis and the Y-axis on the horizontal plane respectively. The final automatic flight of the aircraft[6].

IV. FIXED HEIGHT FUNCTION

The height control adopts the method of double closed loop PID control. When the four-rotor is flying normally, the sensor suddenly encounters external interference, which will cause the sensor to collect data distortion and solve the error height. Only when the height is single-closed, the system is difficult to operate stably. Therefore, the introduction of the z-axis acceleration loop as the inner loop for PID control can effectively avoid the influence of external interference and enhance the robustness of the system.

The output of the PID is the throttle value, the throttle is given the electronic governor value, and the electronic governor controls the motor to make the space three-axis Euler angle and height change.

$$AngelPIDout(t) = k_p e(t) + k_i \sum_{j=0}^{t} e(j)T + k_d \left[e(t) - e(t-1) \right] / T \quad (1)$$

$$AngelRatePIDout(t) = k_p' e'(t) + k_i' \sum_{j=0}^{t} e'(j)T + k_d' \left[e'(t) - e'(t-1) \right] / T \quad (2)$$

The PID control algorithm uses positional digital PID control. Equation (1) is the height loop PID formula, formula (2) is the acceleration loop PID calculation formula, AngelPIDout(t) is the height loop PID output, and AcceleratePIDout(t) is the acceleration loop PID output. e(t)=desired height-actual height, e′(t)=AltitudePIDout(t)-(z-axis acceleration-gravity acceleration value).

The PID output value is first subjected to limiting processing and then output to the throttle to prevent the output throttle value from being too large at some moments, causing overshoot and making the system difficult to stabilize. By continuously adjusting the kp,ki ,kd,kp' ,ki' ,kd' , and six parameters and testing on a quadrotor, a set of values is obtained that allows the aircraft to fly at a steady altitude[7-10].

V. FIXED POINT FUNCTION

Perform cascade PID control of the position loop and speed loop in the horizontal plane. The so-called cascade control uses two controllers to work in series. The output of the outer loop controller is used as the set value of the inner loop controller. The output of the inner loop controller is used to operate the control valve, so that the controlled amount of the outer loop has more Good control effect. This design uses the position loop and the speed loop to control the aircraft horizontally.

First, the optical flow data needs to be processed. In the first step, a simple low-pass filtering is performed on the integral displacement. In step 2, the attitude angle is used to compensate for the integral displacement. In the third step, the integral displacement is differentially processed to obtain the velocity. In step 4, the data unit is converted to centimeters. At this point, the processing of the optical flow data is basically completed. With the two parameters of the integral displacement and the differential speed, the cascade PID control of the position loop and the speed loop in the horizontal plane can be performed.

In the optical flow control, the outer ring performs position control to calculate the target speed to the inner ring, the inner ring performs speed control, calculates the target angle, debugs the first speed loop and then debugs the position loop, and finally compensates, that is, the angle compensation of the above integral displacement is obtained. The position that is not affected by the posture, so far the fixed point function is realized[11-13].

VI. QUADROTOR FLIGHT TEST

According to a recent study by IHS Markit, flying under ideal conditions without additional load, nearly 50% of the drones on the market have an expected battery life of less than 30 minutes, and 35% of the drones have a flight time of 31 to 60 minutes. The remaining 15% and fewer drones can fly for more than an hour. Stelios Kotakis, senior analyst for data transmission and management services at Ihs Markit, said: "Time-of-flight has always been the biggest design challenge for recreational quadcopters and professional drones, especially for those used by companies for over-the-horizon operation. This is especially true for aircraft. The courier company wants drones to have longer battery life and is testing drones to determine the use of drones."

Thus, the life of the aircraft is critical to the indoor stable aircraft system designed for this project. Endurance test of the aircraft designed for this:

Table 1 Endurance test of the aircraft

No-load weight:2.11kg	total weight	Starting battery voltage	duration
Test1	2.11kg	12.4v	6min24s
Test2	2.11kg	12.4v	6min20s
Test3	2.11kg	12.4v	6min20s
Gain weignt to:2.40kg	total weight	Starting battery voltage	duration
Test1	2.40kg	12.4v	6min02s
Test2	2.40kg	12.4v	6min05s
Test3	2.40kg	12.4v	6min07s
Gain weignt to:2.80kg	total weight	Starting battery voltage	duration
Test1	2.80kg	12.4v	5min20s
Test2	2.80kg	12.4v	5min27s
Test3	2.80kg	12.4v	5min22s

In this design, the flight requirements are basically met. To increase flight time, you can reduce the load capacity or increase the battery capacity.

VII. SUMMARY AND OUTLOOK

The existing UAVs are mostly manually controlled indoors, which is highly dependent on the skill level of the operator.

This design adopts open source flight controller, builds a fixed-height flight module based on ultrasonic pen sensor, and a fixed-point module based on optical flow sensor. Multi-sensor fusion can be used when GPS signal, wireless positioning signal and other common positioning signals cannot be effectively used— - that is, indoor flight, precise control of the aircraft, to achieve fixed-point fixed tracking and obstacle avoidance and other functions. At this point, not only the stability of the aircraft is guaranteed, but also the level requirements for the operator are reduced, automatic control is realized, and the popularity of the aircraft can be realized for the consumers rather than the special groups.

In this design, the demand for fixed-point fixed-point flight in indoor environment is met. It is expected to be used in indoor aerial photography, indoor search and rescue, indoor monitoring, indoor patrol, short-distance delivery and aircraft handling training.

The successor can optimize the fixed-point fixed-point mode to make it more stable and reliable, or to increase obstacle avoidance and other functions. I hope that many people will read this article.

References

[1] Xiao Zhicai, Jiang Peng, Dai Hongde, Kang Yuhang. Research Status and Key Technologies of Positioning and Navigation for Indoor Quadrotor Unmanned Aerial Vehicles[J]. Aerospace Missile, 2014, (08): 25-29.

[2] Fei WANG,Jin-Qiang CUI,Ben-Mei CHEN,Tong H LEE. A Comprehensive UAV Indoor Navigation System Based on Vision Optical Flow and Laser FastSLAM[J]. Acta Automatica Sinica,2013,39(11):.

[3] B. C. Min, C. H. Cho, K. M. Choi, D. H. Kim. Development of a Micro Quad-Rotor UAV for Monitoringan Indoor Environment [M]. Springer Berlin Heidelberg: 2009-06-15.

[4] Li Shuaiyang, Wu Lingyu, Zhang Changmao, Ma Zhongli. Research on indoor autonomous hovering of miniature quadrotor based on multi-sensor [J/OL].:1-6(2017-03-27).

[5] Mas, Zhou Tianhong, Liu Fubin, et al. Spin-stabilization and steady-state stable flight of a four-rotor aircraft[J]. Digital Communications World, 2015(12).

[6] Lü Pin, Lai Jizhou, Yang Tianyu, Liu Jianye, Zhu Bin, Song Yifan. Autonomous Navigation Method for Four-Rotor Aircraft Based on Aerodynamic Model[J]. Acta Aeronautica Sinica, 2015, 36(04): 1275-1284

[7] Chen Xiaolong, Tang Qiang, Che Jun, Liu Lin. Indoor Positioning and Control of Four-Rotor Aircraft Based on Artificial Vision[J]. Ordnance Industry Automation, 2012, 31(05): 61-64.

[8] Yu Tuo. Indoor positioning system for four-rotor aircraft [D]. Shanghai Jiaotong University, 2015.

[9] Zhang Yufei, Shen Xingxin. Overall Design of Four-rotor Airborne Robot System for Unknown Indoor Energy

Autonomous Obstacle Avoidance Based on STM32[J]. Science & Technology Communication, 2016, 8(02): 184-185.

[10] Wei Qingtong. Positioning and control of four-rotor UAV based on SLAM in indoor environment [D]. Nanjing University of Aeronautics and Astronautics, 2016.

[11] Hao Wei. Research on task-based indoor adaptive navigation method for quadrotor aircraft [D]. Civil Aviation University of China, 2014.

[12] Dou Huiyang. Design and implementation of obstacle avoidance, cruise and heat source tracking in UAV [D]. Inner Mongolia University, 2017.

[13]Mas, Zhou Tianhong, Liu Fubin, et al. Spin-stabilization and steady-state stable flight of a four-rotor aircraft[J]. Digital Communications World, 2015(12).

Compressed Sensing Based Audio Sampling and Wireless Transmission System

Zhan Hongyan；Shang Yuhan；Wang Kaikai；WangYuan

（Jilin University,College of Instrumentation &Electrical Engineering,Changchun 130021,China）

***Abstract*—Based on the theory of compressed sensing, taking STM32F103 microcontroller as the core of control, a system capable of sampling acoustic signals far below the Nyquist sampling rate is designed, which greatly reduces the requirements on hardware storage capacity and sampling rate and reduces. At the same time, the burden of wireless transmission is reduced. The compressed sampling technology is used to obtain the effective information of the audio signal, and the effective information is transmitted to the host computer terminal for reconstruction and analysis in real time through the nRF24L01 wireless transmission module and the serial port. The experimental results show that the system has good reconstruction effect and low power consumption and high efficiency. It is suitable for occasions requiring long-term sound monitoring.**

***keywords*—Compressed sensing, STM32F103VET6, Wireless transmission**

I. INTRODUCTION

THE traditional signal method acquisition follows the Nyquist law, but the data collected according to this law contains a lot of redundant information, which will cause waste of resources. Compressed sensing was proposed as a new signal acquisition theory in 2006 [1]. Once proposed, this theory has received great attention in the fields of signal processing, magnetic resonance imaging, and wireless communication. The theory of compressed sensing mainly includes three aspects: the sparse representation of the signal, the observation matrix, and the reconstruction algorithm. The theory points out [2]that if the signal has only a small number of non-zero values on a certain transform base, the signal is said to be sparse. For this signal, an observation matrix which is irrelevant to the transform base can be projected onto the low-dimensional space, and the original signal can be reconstructed more accurately by solving the optimization problem.

This design utilizes compressed sampling to compress data during signal acquisition. The sampling frequency is much lower than the Nyquist frequency. The advantage is to reduce the amount of data storage, reduce the hardware performance requirements, and speed up data transmission efficiency. The gradient projection algorithm is used to reconstruct the signal, which has the characteristics of good reconstruction effect, low computational complexity and easy implementation. Combined with the fast and effective working mode of modern people, the human-computer interaction interface was designed to realize real-time operation, real-time measurement, and fast upload and processing of data.

II. OVERALL SYSTEM DESIGN

The system uses the piano music synthesized by MATLAB as the original audio. The signal has sparse characteristics. The observation matrix is used to compress and sample the signal, and a small number of observations are obtained. The gradient reconstruction algorithm is used for audio reconstruction, that is, the l1 norm minimization problem is solved [3], thereby achieving the original signal with a small number of observations.

The system designed in this paper uses STM32F103VET6 as the controller, uses the sound sensor to collect the acoustic signal, and uses the microphone amplifier module and the conditioning circuit to amplify and process the acoustic signal. The analog-to-digital converter converts the processed analog acoustic signal into a digital signal. The timer interrupt mode implements random unequal interval sampling, that is, compressed sampling in the system, and transmits data containing audio effective information to the terminal through wireless transmission and serial communication. The system

block diagram is shown in Figure 1.

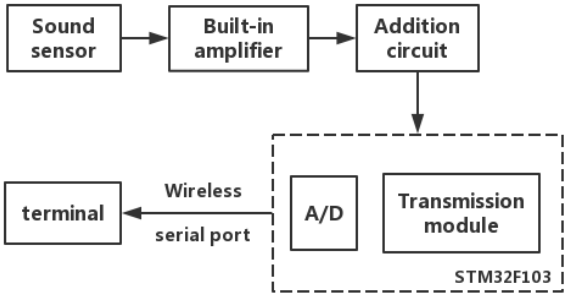

Fig.1 System principle block diagram

III. HARDWARE DESIGN

A. Minimum system selection

This system uses STM32F103VET6 model MCU. The chip has low power consumption, large on-chip storage capacity, high cost performance, and is suitable for engineering selection. In this system, it mainly realizes the function of sound signal A/D sampling and data transmission. The chip includes three 12-bit ADCs with 16 channels, high digital precision, 512k Flash and 64k SRAM, providing enough storage space, two advanced timers and two basic timers for easy time interval generation. Sampling signal. In communication mode, it has SPI and USART, which is convenient for wireless and serial communication design.

B. MAX9812 Microphone Amplifier

The MAX9812 microphone amplifying module is mainly composed of a condenser microphone, a MAX9812 amplifying circuit and an adding circuit, which respectively realize the conversion of the acoustic signal from the physical quantity to the electric quantity, the amplification of the electric quantity and the overall lifting of the voltage.

Commonly used microphones mainly include moving coil microphones and electret condenser microphones. The dynamic microphone uses the principle of electromagnetic induction, which has good sound quality, but is bulky and costly. The condenser microphone is composed of capacitor, DC power supply and load resistor, and its stability, reliability, shock resistance and frequency characteristics are better. In addition, it is small in size, high in sensitivity, and low in cost, so it is suitable for use in this system [4].

The MAX9812 is a single/dual input, 20dB fixed gain microphone amplifier. Its small package size, built-in low-noise microphone paranoia, gain bandwidth product of 500kHz, output up to full swing. It has an extremely low THD+N (0.015%) and, in addition, its supply current is only 230 μ m, and the current is reduced to 100nA in the overall shutdown mode, which meets the low power requirements.

The output characteristics of the MAX9812 microphone amplifier are: when there is no sound, the output voltage is 0. When there is sound, the output voltage is positive and negative, mostly between -1.5~1.5V, and the voltage input range of the A/D conversion circuit of STM32F103VET6 It is 0~3.3V, so it is necessary to add an adding circuit before the A/D conversion, and raise the voltage of the amplifier output to 1.5V as a whole, so that it can be in the range of 0~3V, so that A/D conversion can be performed to obtain digital quantity. The actual voltage signal is restored by subtracting 1.5 from each digital quantity before reconstructing the acoustic signal.

C. nRF24L01 wireless communication module

The nRF24L01 is a single-chip wireless transceiver chip that operates in the ISM band. Its output power, channel selection and protocol settings can be set via the SPI interface. The nRF24L01 has a very low current consumption: 9mA for a transmit power of -6dBm in transmit mode and 123mA for receive mode, and lower current consumption in power-down mode and standby mode. This performance can extend chip runtime.

The pin connection diagram of the wireless transmission module and the STM32F103VET6 microcontroller is shown in Figure 2.

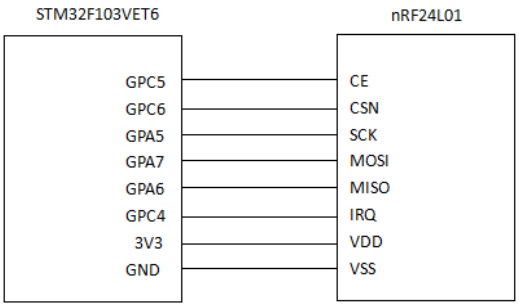

Fig.2 Pin connection diagram

IV. SOFTWARE DESIGN

A. Compressed sampling technique

a) Original audio synthesis

The system uses MATLAB synthesized piano music as the original audio， which is played and then captured by a microphone. The duration of each synthesized note is 0.25s, and the sampling frequency is 44100Hz, that is, the number of samples in the 0.25s' note is 11025. The frequency f of each scale of the piano can be calculated by the "twelve averaging law", and the tone of the corresponding scale can be obtained by adding an exponential envelope[5] to the sine wave of frequency *f*.

b) Compressed sampling process

The sampling process of compressed sensing is different from the traditional Nyquist sampling process. In the process of compressed sampling, the original signal x itself is not directly oversampled, but the signal is obtained through the observation matrix, and the sampling process can be expressed as

$$y = Rx.$$

Where y is the observed value, R is the observation matrix, and x is the original signal.

The characteristics of the observation matrix R are:

1)The number of rows m is equal to the number of sampling points of the compressed sampling, and its value is 8000 in this system;

2)The number of columns n is equal to the original audio time multiplied by the sampling frequency f_s;

3)The number of columns is much larger than the number of rows;

4)There is only one element with a value of 1 and others 0 in each row of the matrix;

5)Elements with a value of 1 have different column values; the column value of the element with a value of 1 in the i-th row is denoted as Ni, the values of N_1 to N_m are randomly generated between 1 and n, without repetition.

The process of compression sampling can be represented by the graphical method, as shown in Figure 3.

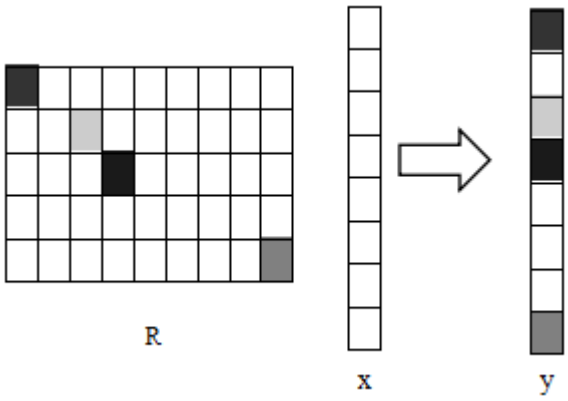

Fig.3 Compressed sampling process schematic diagram

In Figure 3, the observation matrix R has grayscale grids, indicating that the value at this position in the matrix is 1. The original signal x is divided by equal intervals of $1/f_s$ seconds. The gray-scale grid on the observed signal y indicates sampling at the corresponding time, while the white grid indicates no sampling at the corresponding time, thus implementing the compressed sampling process.

c) Compressed sampling method

As long as the different time intervals between the sampling moments are obtained, the microcontroller can be used to sample after different time intervals in actual applications, thereby implementing the compressed sampling process. In this system, the specific method of this process is to transform the observation matrix into an observation array named *measurement*, whitch stores different time intervals in order. This transformation process is described as follows:

The number of points generated in a second when synthesizing the original audio multiplied by the synthesized original audio time is recorded as n. Randomly generate 8000 (sampling points) numbers from 1 to n without repetition using functions in matlab, and sort the 8000 numbers from small to large to get an array S;

Build a matrix *Time* and

$$\begin{cases} Time(1) = S(1), \\ Time(i) = S(i) - S(i-1), i \geq 2 \end{cases}$$

Build a matrix *Timestep_5us* and

$$Timestep\_5us(i) = \mathrm{round}\left(\frac{Time(i) \times 10^6}{5 f_s}\right)$$

Obtain the sampling interval in units of 5

microseconds and round up;

Save the row matrix Timestep_5us as an array in the array *measurement*.

In this system, the interrupt timimg is set to 5us, the array *measurement* is set, the array *buffer* and variables *counter* and *num* are set to save the A/D converted data sequentially. Here, the variable *counter* is used to determine whether the time to acquire the acoustic signal is reached, and the variable *num* is used for the array subscript. The interrupt function program is listed below:

```
void TIM1_UP_IRQHandler(void)
{
if (TIM_GetITStatus(TIM1, TIM_IT_Update) != RESET)//receive an interrupt
{
if (counter<sparse[num]) //insufficient interval
counter++;
else
//specified sampling time
{
    buffer[num]=Get_Adc(10);
//sample
counter=0;
//clear timing
num++;}
//update interval
TIM_ClearFlag(TIM1, TIM_IT_Update );
}
}
```

In this way, compressed sampling can be realized, and the valid data collected is stored in the array buffer in chronological order.

B. ADC digital-to-analog conversion design

The STM32F103VET6 has three 12-bit ADCs. The ADC1 is connected to the APB2 (72MHz). The ADC prescaler provides a clock frequency of up to 12MHz. Since the A/D conversion is performed in the interrupt, in order to minimize the influence on the accuracy of the time interval, the system requires a fast conversion speed and 12 MHz is directly used. Set channel 10 as the ADC1 conversion channel in the program. The sampling time is 1.5 cycles, then the total conversion time of the ADC is equal to sampling time plusing 12.5 cycles, which is 14 cycles. So the conversion time is equal to 14/12, which is 1.17 microseconds. The data is fetched without the form of a function call, but in the form of a direct register operation. Experiments show that 3us is required when using the function call form, and only 1.62us is required when using the register operation.

C. Wireless transmission design

Since the time for wirelessly transmitting one data is greater than the interrupt timing of 5 us, in order to make sure that wireless transmission have no effect on compressed sampling, the system is designed to wirelessly transmit after the end of compressed sampling. The specific method is to turn off the timer after collecting 8000 data, and then the host runs a program for initializing the wireless transmission module and establishes communication with the slave to realize wireless transmission.

At the time of host sampling, the slave has completed initialization of the wireless transmission module and waits for a connection with the host. Waiting for the host acquisition process to end, the slave transmits the data received each time to the terminal through serial communication after connected with host.

V. TEST RESULTS

As shown in Figure 4, the near side is a host for compressed sampling and transmitting data, and the far side is a slave and a terminal for receiving and processing data.

In order to verify the reconstruction effect of the system, a piece of 14.5s audio containing synthetic piano music is played and 8000 data is collected and transmitted to the host computer for processing. The processed result is shown in Figure 5, where green curve is the synthesized original sound signal, and red curve is the reconstructed signal after compression sampling. After performing Fourier transform on these two signals respectively, it is found that their spectral coincidence degree is high. After analysis, the system reconstruction effect is better.

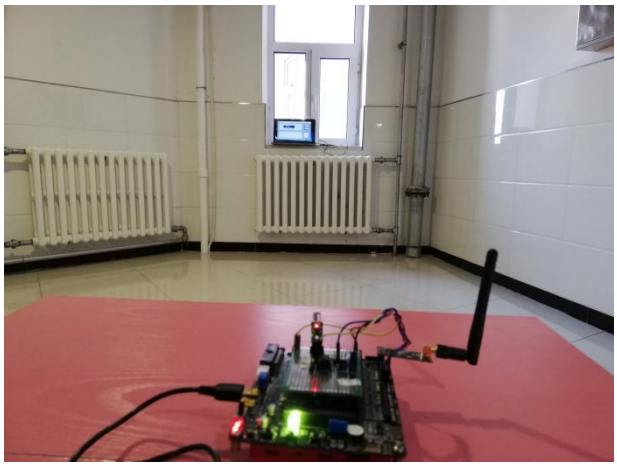

Fig.4 System hardware display diagram

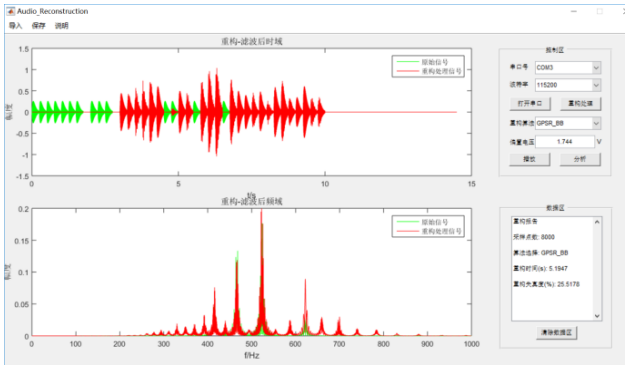

Fig.5 Audio reconstruction analysis results

VI. CONCLUSION

Actual test results show that compressed sensing based audio sampling and wireless transmission system can still achieve better reconstruction of the sound signal in the case where the amount of sampled data is only 1/160 of the amount of collected signal data at the standard sampling frequency. Since the theory of compressed sensing has been proposed in 2006, its application in the audio field is far less than that in image processing. The system converts the theory of audio compression perception into practice and has certain application value.

References

[1] Donoho D. Compressed sensing [J]. IEEE Transactions on Information Theory,2006, 52(6): 1289-1306.

[2] Wang Shaomin. Research on Signal Reconstruction Algorithm Based on Gradient Projection in Compressed Sensing [D]. Northeastern University, 2011.

[3] M. A. T. Fiqueiredo, R. D. Nowak, S. F. Wright. Gradient projection for sparsereconstruction: Application to compressed sensing and other inverse problems [J].IEEE Journal of Selected Topics in Signal Processing, 2007, 1(14): 586 -598.

[4] Cui Xingmei. Audio Signal Processing and Application Based on Compressed Sensing [D]. Nanjing: Nanjing University of Science and Technology, 2016.

[5] Li Min, Zhang Weiwei, Jiang Minxin, Liu Yan. Music Analysis and Synthesis Experiment Design Based on MATLAB [J]. Journal of Dalian Nationalities University, 2010,12(03):269-271.

The design of charging control device based on mobile phone monitoring

Chen Yihan；Xiang Menghang；Wu Zheng

（Jilin University,College of Instrumentation &Electrical Engineering,Changchun 130021,China）

***Abstract*— The modern society has made continuous progress in science and technology, and electronic digital products have developed rapidly. People's dependence on portable electronic products such as mobile phones, laptops, and smart wearable devices has gradually increased[1]. While the equipment with high performance and high configuration provides convenience for people's work and life, the problems in the charging process are also exposed. The device adds a module for monitoring the charging data so that the user can know the charging status in real time from the charging display or remotely. The device body is provided with an environmental data detecting circuit to remotely feedback the environmental conditions such as temperature and humidity of the charging process to the user, so that the user can grasp the charging environment around the device[2-5].**

***keywords*—Charging Monitor Environment**

I. INTRODUCTION

THE design of the charging control device based on mobile phone monitoring is mainly for the research and design of thin and light business notebooks such as tablet PC and Apple Mac[6-7]. It is designed by hardware system (multiple magnetic power cord, DC voltage and current adjustable circuit, charging data collection module\Wi- Fi module) and software system (mobile phone software application).

The device adopts the "Internet +" combination of software and hardware, collects data through hardware, collects and processes data locally, and displays terminal intelligent software to achieve close connection between online and offline[8-10].

II. SYSTEM DESIGN

The design idea of the charging device based on mobile phone monitoring: This design is controlled by the core board of STM32F103C8T6 single chip microcomputer. The whole circuit is composed of five parts: charging circuit, control circuit, monitoring circuit, LCD display circuit and Bluetooth module circuit. The monitoring circuit includes a voltage, a current monitoring circuit, and a temperature and humidity monitoring circuit[11].

III. CHARGING CIRCUIT DESIGN

This design firstly realizes the output range of 5V~35V voltage through the XL6009 boost module through DC power supply to charge the device. The overcharge protection and current control of the device are realized by the control signal of the single chip microcomputer [12].

The schematic diagram of the XL6009 boost module circuit is shown in Figure 1. It is mainly composed of XL6009 step-up DC power converter chip, diode and inductor and capacitor. Among them, the 3-pin of the step-up DC power converter chip of the XL6009 is used as a square wave output signal.

When the 3-pin output shows a low level, due to the diode's single-conductivity, D1 is turned off, and the inductor L1 acts as an energy storage component to store the voltage. At this time, the capacitors C1 and R1 form a loop discharge, causing the output voltage to drop; When the 3-pin output shows a high level, the same reason, D1 is turned on at this time, the inductor L1 charges to both ends of the capacitor, and the output voltage rises[13].

R1 and R2 are voltage amplifiers built into the XL6009 chip. The output voltage is stabilized by negative feedback. The voltage amplification can be controlled by resistors R1 and R2 [3].

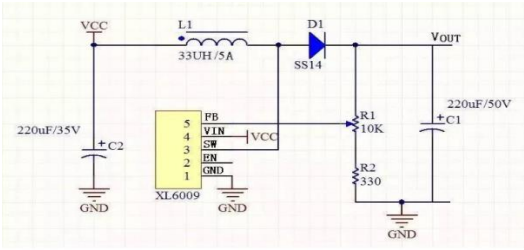

Figure 1 Boost module circuit schematic

IV. MONTIORING CIRCUIT DESIGN

In order to ensure the safety of the equipment during the overall charging process, important parameters of the charging process must be monitored in real time.

In addition to considering the complexity of the charging environment and the adaptability of smart devices, the device also incorporates temperature and humidity.

Data such as current, voltage and power are collected and processed and displayed on the device in real time. ACS712 current detection module to achieve real-time monitoring of the charging circuit [4] as shown in Figure 2[14].

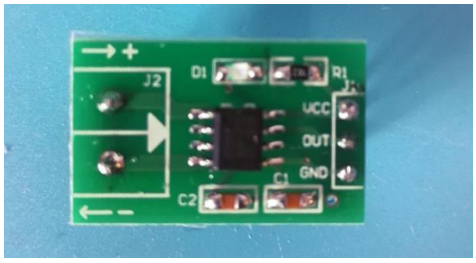

Figure 2 ACS712 current detection module

In order to verify its function, we searched the lithium battery of the common mobile phone model on the market for voltage and current testing. The measured data are shown in Table 1.

Table 1 Voltage and Current Power Data

Voltage(v)	4.1	4.1	4.1	4.1	4.1	4.1	4.1
Current(I)	0	0	0	0	0	0	0
Voltage(v)	4.1	4.1	4.1	4.1	4.1	4.1	4.1
Current(I)	0	0	0	0	0	0	0
Voltage(v)	4.2	4.2	4.2	4.2	4.2	4.2	4.2
Current(I)	0	0	0.17	0.16	0.12	0.15	0.15

In addition, we also used a thermometer to compare the measured temperature with the sensor display. The data comparison chart is shown in Figure 3.

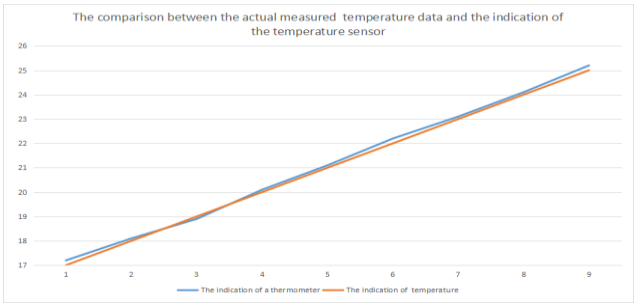

Figure 3 Contrast Diagram between Temperature and Sensor

Finally, the hygrometer is used to check the measured humidity and the sensor display. The data comparison chart is shown in Figure 4.

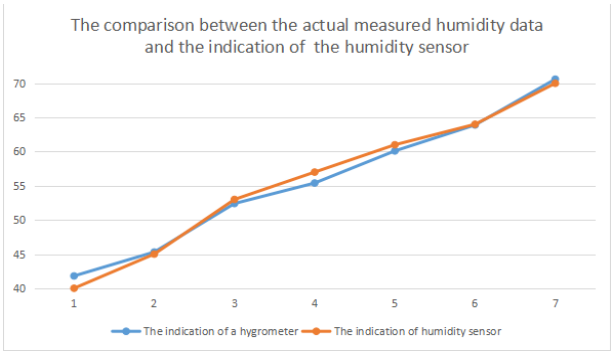

Fig.4 Contrast Diagram between Measured Humidity and Sensor Indicator Data

V. DISPLAY CIRCUIT DESIGN

The data acquisition display circuit comprises two parts: a data acquisition end LCD display system and a mobile display end. The LCD display directly controls the output display through the microcontroller. The mobile terminal communicates with the mobile phone device through the Bluetooth module, and displays various data in real time on the app [15].

VI. IN CONCLUSION

In this paper, a charging device based on mobile phone monitoring is designed. The data collected by the sensor is displayed and transmitted in real time, so that the user can clearly know the current state of charging and provide a certain guarantee for charging the device.

References

[1] Sha Zhanyou, Pang Zhifeng, Zhang Suying. Circuit design of cell phone battery constant current/constant power charger [J]. Electrical measurement and instrumentation, 2001, 38 (5): 31-33.

[2] Liu Meizhun. Design of general intelligent charger based on single chip computer [J]. Instrument technology and sensors, 2006, 9:41-43.63.

[3] Fangping, prosperous Zhou. Design of simple universal charger [J]. Electronic production, 2013, 8X: 6-6.

[4] He Limin. Selected 1/2/3 of SCM application technology [M]. Beijing: Beijing University of Aeronautics and Astronautics Press, 1992.

[5] Xie Zusen. Development and Typical Application Design of Single Chip Microcomputer [M]. Beijing: Machinery Industry Press: 9, 1997.

[6] Bodson D. One-Size-Fits-All Mobile Phone Charger [Standards][J]. IEEE Vehicular Technology Magazine, 2011, 6(3): 107-110.

[7] Qu A D, Zhang Z H. The Design of Charger based on 1T SCM[C]//Applied Mechanics and Materials. Trans Tech Publications, 2013, 347: 1553-1556.

[8] Kim C G, Seo D H, You J S, et al. Design of a contactless battery charger for cellular phone[J]. IEEE Transactions on Industrial Electronics, 2001, 48(6): 1238-1247.

[9] Ziadi Y, Qjidaa H. A High Efficiency Li-Ion Battery LDO-Based Charger for Portable Application[J]. Active and Passive Electronic Components, 2015, 2015.

[10] Li X Z, Hu G M, Hou P X, et al. Analysis on Harmonics Caused by Connecting Electric Vehicle Chargers with Power Network[C]//Advanced Materials Research. Trans Tech Publications, 2013, 724: 1393-1397.

[11] (U.S.) D.H. Shi Kai-shek, Xu Debing Translated Sensor Interface and Signal Conditioning Circuit [M]. Beijing: National Defense Industry Press, 1984.1.

[12] Liu Meizhun. Design of general intelligent charger based on single chip computer [J]. Instrument technology and sensors, 2006, 9:41-43.63.

[13] Yang Xingqiang, Sun Guoliang. An Intelligent Charging System for Mobile Phone Battery Based on Single Chip Microcomputer [J]. Journal of Nanyang Normal University, 2009, 8 (12).

[14] Zhang Haiwang, Yang Bo. Application of Cloud Computing in Mobile Communication [J]. Computer Security, 2011: 49-51.

[15] Sha Zhanyou, Pang Zhifeng, Zhang Suying. Circuit design of cell phone battery constant current/constant power charger [J]. Electrical measurement and instrument, 2001, 38 (5): 31-33.